Control of Axial–Torsional Dynamics of a Distributed Drilling System

Mohammad Amin Faghihi, Shabnam Tashakori, Ehsan Azadi Yazdi, Hossein Mohammadi, Mohammad Eghtesad, and Nathan van de Wouw, *Fellow, IEEE*

***Abstract*— Self-excited vibrations in drill-string systems are one of the main causes of failure and efficiency reduction in drilling operations. To suppress these vibrations, an active control strategy is proposed in this article based on a distributed drill-string model. Herein, the coupled axial–torsional dynamics of the drill string are taken into account. This coupling takes place through the bit–rock interaction, consisting of the cutting and the frictional components. The drill-string model is expressed as a neutral-type delay differential equation (NDDE) with constant and state-dependent state delays and constant input delays. As a first step in the novel controller design, a compensator is designed to mitigate the reflective waves at the top side of the string, which, in turn, results in the elimination of the neutral terms and some of the constant time delays in the delay system model. This supports a simplified next step of stabilizing controller design. Second, a new method is proposed to provide sufficient conditions for exponential stability with a prescribed minimal transient decay rate. Based on these conditions, a parametric feedback control law is designed. Finally, to make the controller causal, a predictor is designed which predicts the future state by only employing top-side measurements, available in practice. A simulation-based case study reflecting real-life scenarios is presented to illustrate the effectiveness of the proposed controller. It is also illustrated that the controller is robust against parametric uncertainties and measurement noise.**

***Index Terms*— Distributed drill-string dynamics, input delay, neutral-type time delay (NTD) model, prediction-based control, state-dependent delay.**

I. Introduction

DRILL-STRING systems used to explore and harvest (geothermal) energy, and mineral resources, and for CO_2 storage, suffer from self-excited oscillations during operation. Complex coupled dynamics, including torsional, axial, and lateral vibrations, can cause detrimental phenomena such as stick–slip, bit-bounce, or whirling which lead to drilling efficiency reduction, increased system downtime, and system failure. Consequently, an effective control strategy, either passive or active, is required to mitigate such vibrations.

The main sources of such drill-string vibrations are the bit–rock interaction, fluid–structure interaction between the drilling mud and the drill string, and impact between the drill string and the borehole wall [1], [2], [3]. This article focuses on vibrations caused by the interplay between the bit–rock interaction and infinite-dimensional dynamics of the drill string.

Different approaches have been employed to model the bit–rock interaction in drilling systems. Experiments indicate that the reactive torque on bit (TOB) decreases when the bit angular velocity increases [4]. This feature, which is called the velocity-weakening effect, was initially considered as an intrinsic characteristic of the friction forces between the bit and the formation [5], [6], [7]. However, experiments do not reveal any intrinsic velocity-weakening effect [4]. In [4], it was demonstrated that interaction forces between formation and poly-crystalline diamond compact (PDC) bits consist of a cutting process and a frictional contact process. Cutting forces have a positive correlation with the depth-of-cut, which in turn depends on the current and the previous axial positions of the drill bit. This dependence on the present and the previous states is called the regenerative cutting effect [8]. The corresponding time delay depends on the angular velocity of the bit. Hence, the time delay, which is introduced by the regenerative cutting effect to the equations of motion, is state-dependent. The regenerative cutting effect is known as the root cause of instability and self-excited oscillations in the coupled axial–torsional dynamics of drilling systems. The aforementioned state-dependent delay model formulation has been employed to study the drill-string vibrations in [9], [10], [11], [12], [13], [14], [15], [16], and [17]. In the presence of severe self-excited oscillations, the cutting blades may lose contact with the formation. This causes multiple regenerative effects, which introduces several state-dependent time delays to the equations of motion (rather than only one state-dependent time delay) [18], [19].

To model the dynamics of the drill string, several approaches have been employed: lumped-parameter models [14], [15], [20], [21], [22], [23], finite element models [16], [24], [25], [26], distributed parameter models [13], [27], [28], and

Manuscript received 26 April 2023; revised 6 May 2023; accepted 1 July 2023. Date of publication 4 August 2023; date of current version 29 December 2023. Recommended by Associate Editor J. B. Hoagg. *(Corresponding author: Hossein Mohammadi.)*

Mohammad Amin Faghihi, Ehsan Azadi Yazdi, and Hossein Mohammadi are with the Department of Mechanical Engineering, Shiraz University, Shiraz 71348-14336, Iran (e-mail: amin.faghihi@hafez.shirazu.ac.ir; ehsanazadi@shirazu.ac.ir; h_mohammadi@shirazu.ac.ir).

Shabnam Tashakori is with the Department of Mechanical Engineering, Shiraz University of Technology, Shiraz 71557-13876, Iran (e-mail: tashakori@sutech.ac.ir).

Mohammad Eghtesad, deceased, was with the Department of Mechanical Engineering, Shiraz University, Shiraz 71348-14336, Iran (e-mail: eghtesad@shirazu.ac.ir).

Nathan van de Wouw is with the Department of Mechanical Engineering, Eindhoven University of Technology, 5600 MB Eindhoven, The Netherlands (e-mail: n.v.d.wouw@tue.nl).

Digital Object Identifier 10.1109/TCST.2023.3298255

neutral-type time delay (NTD) models [23], [29], [30]. The NTD model, obtained from the d'Alembert's solution for the wave equation, represents the infinite-dimensional drill-string dynamics. Since the distributed elastic nature of the drill string is considered in the NTD model (as a platform for propagating waves), it is more comprehensive than lumped-parameter models. Moreover, a greater variety of stability analysis and control methods are available for such NTD models in comparison with models formulated by partial differential equations (PDEs) [31]. However, these NTD models are representative of the underlying PDE dynamics if the damping effects along the drill string are negligible. According to the finite speed of the propagating waves, a delay is introduced to the control inputs since the control signals must travel from the top to the bottom of the drill string to reach the bit.

There have been several attempts to address the problem of input delays. In order to compensate for input delays, the well-known Smith predictor has been proposed in [32]. Based on this scheme, several studies have been devoted to solving control problems with input delays [31], [33], [34], [35]. Later, research extended to systems with both input and state delays [36], [37], [38]. It is demonstrated that the above-mentioned methods are practically unstable with high-frequency modes [39], [40], [41]. This problem can be solved by adding a low-pass filter to the control input [42]. This approach is employed in [43] to develop an implementable predictor design methodology for systems with state delays and several input delays. The drill-string system dynamics presented in this article fall into this category, as it consists of the bit–rock interaction law inducing (state-dependent) state delays and the NTD model for the drill string introducing constant input and state delays.

Control approaches have been proposed to suppress unwanted vibrations in drilling systems. In these approaches, mostly, some surface variables are considered as control inputs, e.g., the top-driven torque or angular velocity in the torsional direction and the hook force or axial velocity in the axial direction. Active control methods for mitigating coupled axial–torsional vibrations have been employed for lumped-parameter models [11], [44], [45], finite element models [46], [47], distributed parameter models [48], coupled PDE-ODE models [49], and NTD models [50], [51], [52], [53]. However, existing control methods for mitigating coupled axial–torsional vibrations of NTD models have some drawbacks/limitations. The employed bit–rock interaction law in [50] and [51] does not capture the regenerative effect, which is an essential source of instability leading to drill-string vibrations. The proposed controller in [52] has limited robustness according to the existence of unchangeable spectral asymptotes near the imaginary axis, due to the neutral nature of the delay systems dynamics. Furthermore, the control approach is not automated, i.e., the controller should be redesigned if the drill-string design specifications change. Also, [54] and [53] did not take into account the input delay in the controller design, while this delay is indeed one of the significant challenges of the drilling system control problem. In summary, an automated (parametrized) controller for the NTD drill-string models considering both input delays and regenerative cutting effects does not exist in the literature. In addition, the exponential decay rate of the closed-loop system cannot be arbitrarily chosen as a control design specification in the existing control approaches for neutral-type delay differential equations (NDDEs).

In this article, the infinite-dimensional drill-string dynamics are formulated in terms of NDDEs with constant input and constant state delays, corresponding to the required time for the wave to travel along the string, and a state-dependent state delay, corresponding to the cutting process. In comparison with previous studies, the following novel contributions are made.

1) The coupled dynamics presented in [52] is reformulated in terms of a model involving a lower-dimensional state-space. In addition to expressing the system dynamics in a simpler way, which also simplifies the controller design, this reformulation eliminates the need for observer design to estimate unmeasurable states based on top-side measurements.
2) A compensator is designed to mitigate the reflective waves at the top boundary. In this manner, all the delayed terms caused by the wave reflection, especially the neutral delay terms, are compensated for, and the uncompensated part of the dynamics is transformed into simpler retarded delay differential equations (RDDEs). Therefore, this compensator design transforms the controller design problem into a favorable form. Namely, NDDEs have vertical spectral asymptotes, which cannot be changed by state-feedback controllers [55]. Accordingly, the existence of an asymptote in the closed right-half complex plane makes the system not formally stable, i.e., not stabilizable by state-feedback [56]. By using the proposed compensator, even such systems can be rendered as stabilizable systems (by state feedback). Note that suppressing reflective waves in drill strings has been considered in the scope of so-called impedance matching approaches in the literature. However, the existing impedance matching approaches for drilling systems [57], [58] are used for the drill strings with frictional bit–rock interaction models, which only consider the bit–rock interaction as a function of the bit angular velocity and disregard the (regenerative) effect of the depth-of-cut. In this article, a novel approach is developed dealing with both the reflection of traveling waves and the regenerative effect due to the bit–rock interaction.
3) A new method for guaranteeing the exponential stability of the transformed system is developed. In this method, sufficient conditions are presented to ensure a minimal exponential transient decay rate.
4) A novel state-feedback controller is designed (based on the aforementioned conditions), with design conditions formulated in terms of system parameters. The parametric structure of the controller makes it easily applicable to a wide range of drill-string systems with different parameter values. Furthermore, the robustness of the system can be adjusted since the exponential decay rate

of the closed-loop system (the right-most eigenvalue) is a design parameter.

5) A predictor is designed to cope with the delays in the control inputs induced by the finite wave propagation speed of the drill string, causing a delay in the input affecting down-hole variables and in the output measurements (due to the same effect, which causes the sensors at the top drive to measure the effect of vibration at the bit with a delay). The predictor design is extended by a low-pass filter in order to make it implementable.

Moreover, the effectiveness of the proposed predictor-based control approach is illustrated by applying it to a representative case study of a real-life drilling system. The simulation results show that the proposed controller is robust against parametric uncertainties and measurement noise.

This article is organized as follows. In Section II, the distributed model for axial and torsional drill-string dynamics is introduced in a novel lower-dimensional form. Then, the linearized perturbation dynamics are presented. In Section III, the compensator is designed and the stabilizing state-feedback law is presented. In order to make the control law causal, a predictor is proposed in Section IV which is practically implementable by incorporating a low-pass filter in the design. The effectiveness of the designed controller and its robustness against parametric uncertainties and measurement noise are shown by presenting the illustrative simulation results in Section V. Finally, the conclusions are presented in Section VI.

II. Drill-String System Model

In this article, the drill string is considered a continuous rod under axial forces and a continuous shaft under torsional torques. Herein, the following assumptions are taken into account.

1) The material and geometric properties are assumed constant.
2) Internal and external dampings are negligible.
3) Structural nonlinearities, as well as the friction and impact between the drill string and the borehole wall are ignored.

Consequently, the torsional and axial dynamics of the drill string are governed by the following wave equations [13], [27], [29], [51]:

$$\frac{\partial^2 \Phi}{\partial x^2}(x,t) = c_t^2 \frac{\partial^2 \Phi}{\partial t^2}(x,t) \tag{1a}$$

$$\frac{\partial^2 U}{\partial x^2}(x,t) = c_a^2 \frac{\partial^2 U}{\partial t^2}(x,t) \tag{1b}$$

where $\Phi(x,t)$ and $U(x,t)$ are the angular and axial displacements, respectively, which are functions of time t and distance from the top extremity x. The wave constants in (1), c_t and c_a, are defined as follows:

$$c_a = \sqrt{\frac{\rho}{E}} \tag{2a}$$

$$c_t = \sqrt{\frac{\rho}{G}} \tag{2b}$$

where ρ is the density and E and G are Young's modulus and the shear modulus of the pipes, respectively. Physically, c_t and c_a represent the reciprocal of the torsional and axial wave propagation speeds, respectively. The solution of (1) can be defined in terms of Riemann variables as follows:

$$\Phi(x,t) = \eta_t(t + c_t x) + \xi_t(t - c_t x) \tag{3a}$$

$$U(x,t) = \eta_a(t + c_a x) + \xi_a(t - c_a x) \tag{3b}$$

where η and ξ, respectively, represent the up- and down-traveling waves with the subscripts t and a standing for the torsional and axial dynamics. Let us use the prime symbol $'$ to show the derivative of a scalar function with respect to its scalar argument, e.g., $\eta'(s) := (d\eta/ds)(s)$. Differentiating (3) with respect to t and x gives

$$\frac{\partial \Phi}{\partial t}(0,t) = \eta_t'(t) + \xi_t'(t) \tag{4a}$$

$$\frac{\partial \Phi}{\partial x}(0,t) = c_t \eta_t'(t) - c_t \xi_t'(t) \tag{4b}$$

$$\frac{\partial \Phi}{\partial t}(L,t) = \eta_t'(t + \tau_t) + \xi_t'(t - \tau_t) \tag{4c}$$

$$\frac{\partial \Phi}{\partial x}(L,t) = c_t \eta_t'(t + \tau_t) - c_t \xi_t'(t - \tau_t) \tag{4d}$$

and

$$\frac{\partial U}{\partial t}(0,t) = \eta_a'(t) + \xi_a'(t) \tag{5a}$$

$$\frac{\partial U}{\partial x}(0,t) = c_a \eta_a'(t) - c_a \xi_a'(t) \tag{5b}$$

$$\frac{\partial U}{\partial t}(L,t) = \eta_a'(t + \tau_a) + \xi_a'(t - \tau_a) \tag{5c}$$

$$\frac{\partial U}{\partial x}(L,t) = c_a \eta_a'(t + \tau_a) - c_a \xi_a'(t - \tau_a) \tag{5d}$$

where L is the drill-string length, and the time delays τ_t and τ_a are, respectively, the time required for the torsional and axial waves to travel the drill-string length, defined as follows:

$$\tau_t = c_t L, \quad \tau_a = c_a L. \tag{6}$$

The bottom hole assembly (BHA) is the bottom part of the drill string which consists of a stiffer pipe section and the bit. The BHA interacts with the drilling pipes from its top side, and with the formation by means of the drill bit. Accordingly, the following equations of motion govern the BHA/bit, which is considered a rigid part:

$$J_b \Phi_b''(t) = -GJ \frac{\partial \Phi}{\partial x}(L,t) - T(t) \tag{7a}$$

$$M_b U_b''(t) = -EA \frac{\partial U}{\partial x}(L,t) - W(t) \tag{7b}$$

where $\Phi_b(t) = \Phi(L,t)$ and $U_b(t) = U(L,t)$ represent the bit angular and axial displacements, respectively. J is the cross-sectional polar moment of area, A is the cross-sectional area of the string, J_b is the BHA moment of inertia, and M_b is the mass of the BHA. Furthermore, $T(t)$ and $W(t)$ are the applied TOB and weight on bit (WOB) acting on the bit from the formation, respectively. Moreover, the boundary conditions at the top side of the drill string are defined by introducing the top-driven angular velocity $\Omega(t)$ and axial velocity $V(t)$

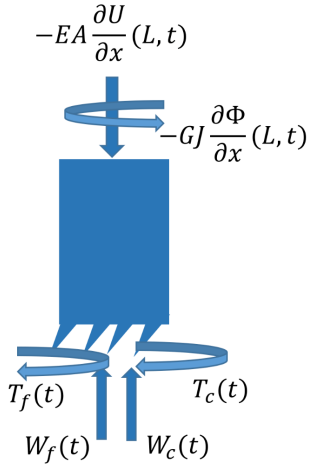

Fig. 1. Schematic of a bit including the force and torque interaction due to the bit–rock interaction (bottom) and the interaction with the drill string (top).

as the control inputs as follows:

$$\Omega(t) = \frac{\partial \Phi}{\partial t}(0,t) \tag{8a}$$

$$V(t) = \frac{\partial U}{\partial t}(0,t). \tag{8b}$$

Torsional and axial equations of motion can be obtained by solving (4), (5), and (7), regarding (8), as a set of algebraic equations (for more details refer to [52]), as follows:

$$\begin{aligned}\Phi_b''(t) - \Phi_b''(t-2\tau_t) = &-\frac{GJc_t}{J_b}\big(\Phi_b'(t) + \Phi_b'(t-2\tau_t)\big)\\ &+\frac{1}{J_b}\big(-T(t) + T(t-2\tau_t)\big)\\ &+\frac{2GJc_t}{J_b}\Omega(t-\tau_t)\end{aligned} \tag{9a}$$

$$\begin{aligned}U_b''(t) - U_b''(t-2\tau_a) = &-\frac{EAc_a}{M_b}\big(U_b'(t) + U_b'(t-2\tau_a)\big)\\ &+\frac{1}{M_b}\big(-W(t) + W(t-2\tau_a)\big)\\ &+\frac{2EAc_a}{M_b}V(t-\tau_a).\end{aligned} \tag{9b}$$

The following bit–rock interaction law is employed to model $T(t)$ and $W(t)$ [14]:

$$T(t) = T_c(t) + T_f(t) \tag{10a}$$

$$W(t) = W_c(t) + W_f(t) \tag{10b}$$

where $T(t)$ and $W(t)$ are composed of the cutting and frictional components, denoted with c and f subscripts, respectively. A schematic of the bit under cutting and frictional bit–rock interaction is depicted in Fig. 1. The cutting and frictional components of the bit–rock interaction are defined as follows [52]:

$$T_c(t) = \frac{1}{2}\epsilon a^2 \mathbf{R}\big(d(t)\big)\mathbf{H}\big(\Phi_b'(t)\big) \tag{11a}$$

$$T_f(t) = \frac{1}{2}\mu\gamma a^2 \sigma l \mathbf{Sign}\big(\Phi_b'(t)\big)\mathbf{H}\big(d(t)\big)\mathbf{H}\big(U_b'(t)\big) \tag{11b}$$

$$W_c(t) = \epsilon a \zeta \mathbf{R}\big(d(t)\big)\mathbf{H}\big(\Phi_b'(t)\big) \tag{11c}$$

$$W_f(t) = \sigma a l \mathbf{H}\big(d(t)\big)\mathbf{H}\big(U_b'(t)\big) \tag{11d}$$

where ϵ is the rock intrinsic specific energy, a is the bit radius, ζ is the cutter inclination number, σ is the maximum contact pressure at the wearflat–rock interface, l is the length of the drill bit wearflat, μ is the coefficient of friction at the wearflat–rock interface, and γ is the bit geometry number. These constant parameters represent the bit–rock interaction properties. Also, $\mathbf{R}(.)$ is the Ramp function, $\mathbf{H}(.)$ is the Heaviside function, and $\mathbf{Sign}(.)$ is the set-valued Sign function [29]. Furthermore, $d(t)$, the depth-of-cut, is given by

$$d(t) = n\big(U_b(t) - U_b\big(t - \tau_n(t)\big)\big) \tag{12}$$

where n is the number of the cutting blades, and $\tau_n(t)$ is the time which takes for the bit to rotate by the angle $(2\pi/n)$, which is determined by using the following implicit relation:

$$\Phi_b(t) - \Phi_b\big(t - \tau_n(t)\big) = \frac{2\pi}{n} \tag{13}$$

which shows the state-dependency of the delay (i.e., the delay τ_n needed in the depth-of-cut depends on the state Φ_b).

A. Linearized Perturbation Dynamics

Consider the drilling operation with constant reference angular and axial velocities at the top drive

$$\Omega(t) = \Omega(t-\tau_t) = \Omega_0, \quad V(t) = V(t-\tau_a) = V_0. \tag{14}$$

Then, the steady-state response of the bit is the bit motion with the same constant angular and axial velocities

$$\Phi_b'(t) = \Omega_0, \quad U_b'(t) = V_0. \tag{15}$$

Indeed, in the steady-state operation, the bit angular and axial velocities are the same as the angular and axial velocities of the top drive. In this case, the whole drill string is rotating and moving with a constant angular and axial velocity. However, the drill string is twisted with a constant angle according to the constant TOB and it is compressed with a constant axial deformation according to the constant WOB. Let us show this claim. Using (15) in (12) and (13) gives the following constant value for the depth-of-cut:

$$d(t) = d_0 := \frac{2\pi V_0}{\Omega_0}. \tag{16}$$

Since $\Phi_b'(t)$, $U_b'(t)$, and $d(t)$ are constant in the steady-state motion, the force and torque components in (11) are constant as well, resulting in constant total TOB and WOB in (10). As a result, in steady-state motion, we have that

$$T(t) = T(t-2\tau_t) = T_0, \quad W(t) = W(t-2\tau_a) = W_0 \tag{17}$$

where T_0 and W_0 are the steady-state TOB and WOB, respectively, given by

$$T_0 = T_{c_0} + T_{f_0} \tag{18a}$$

$$W_0 = W_{c_0} + W_{f_0}. \tag{18b}$$

The steady-state TOB components, T_{c_0} and T_{f_0}, and the steady-state WOB components, W_{c_0} and W_{f_0}, are obtained by substituting the positive constant steady-state angular and

axial velocities from (15), and the positive constant steady-state depth-of-cut from (16) into (11) as follows:

$$T_{c_0} = \frac{1}{2}\epsilon a^2 d_0 \tag{19a}$$
$$T_{f_0} = \frac{1}{2}\mu\gamma a^2 \sigma l \tag{19b}$$
$$W_{c_0} = \epsilon a \zeta d_0 \tag{19c}$$
$$W_{f_0} = \sigma a l. \tag{19d}$$

Substituting $\Omega(t-\tau_t)$ and $V(t-\tau_t)$ from (14), and $\Phi'(t)$ and $V'(t)$ from (15) into (9) and using (17) shows that this steady-state, constant velocity solution indeed satisfies the dynamics in (9). Without loss of generality, we assume that the origin is at the initial position of the bit, i.e., $\Phi_b(0) = 0$ and $U_b(0) = 0$. Accordingly, the steady-state angular and axial displacements of the bit are given by

$$\Phi_b(t) = \Omega_0\, t, \quad V_b(t) = V_0\, t. \tag{20}$$

Of course, when the system is not evolving on this steady-state solution, then (20) is not satisfied. Now, let us define the perturbed variables (with subscript "p") as the deviation of the system state and inputs from the above steady-state response and the constant reference input, respectively, as follows. First, the perturbed top-driven (angular and axial) velocities, i.e., perturbations of the control input with respect to the nominal values, are given by

$$\Omega_p(t) = \Omega(t) - \Omega_0, \quad V_p(t) = V(t) - V_0. \tag{21}$$

Second, the perturbed angular and axial bit displacements and the perturbed depth-of-cut are given by

$$\Phi_p(t) = \Phi_b(t) - \Omega_0\, t, \quad U_p(t) = U_b(t) - V_0 t \tag{22a}$$
$$d_p(t) = d(t) - d_0. \tag{22b}$$

When the perturbed torsional and axial velocities and the perturbed depth-of-cut are less (in magnitude) than the corresponding nominal values, the angular and axial velocities, $\Phi_b'(t)$, $U_b'(t)$, and the depth-of-cut, $d(t)$, remain positive. Hence, under such conditions, the TOB and WOB components in (11) can be rewritten without using the discontinuous and nonsmooth functions, $\mathbf{R}(.)$, $\mathbf{H}(.)$, and $\mathbf{Sign}(.)$, as follows:

$$T_c(t) = \frac{1}{2}\epsilon a^2 d(t) \tag{23a}$$
$$T_f(t) = \frac{1}{2}\mu\gamma a^2 \sigma l \tag{23b}$$
$$W_c(t) = \epsilon a \zeta d(t) \tag{23c}$$
$$W_f(t) = \sigma a l. \tag{23d}$$

Using (23) and (19) with regards to (22b) gives

$$T_c(t) = T_{c_0} + \frac{1}{2}\epsilon a^2 d_p(t) \tag{24a}$$
$$T_f(t) = T_{f_0} \tag{24b}$$
$$W_c(t) = W_{c_0} + \epsilon a \zeta d_p(t) \tag{24c}$$
$$W_f(t) = W_{f_0}. \tag{24d}$$

Substituting $T_c(t)$, $T_f(t)$, $W_c(t)$, and $W_f(t)$ from (24) in (10) regarding (18) gives

$$T(t) = T_0 + \frac{1}{2}\epsilon a^2 d_p(t) \tag{25a}$$
$$W(t) = W_0 + \epsilon a \zeta d_p(t). \tag{25b}$$

As a consequence, only the cutting components of the bit–rock interaction contribute to the perturbed part of the TOB and WOB as follows:

$$T_p(t) = \frac{1}{2}\epsilon a^2 d_p(t), \quad W_p(t) = \epsilon a \zeta d_p(t). \tag{26}$$

Subsequently, the equations of motion in the perturbed coordinates are given by

$$\begin{aligned}\Phi_p''(t) - \Phi_p''(t-2\tau_t) = &-\frac{GJc_t}{J_b}\big(\Phi_p'(t) + \Phi_p'(t-2\tau_t)\big)\\ &+ \frac{\epsilon a^2}{2J_b}\big(-d_p(t) + d_p(t-2\tau_t)\big)\\ &+ \frac{2GJc_t}{J_b}\Omega_p(t-\tau_t)\end{aligned} \tag{27a}$$
$$\begin{aligned}U_p''(t) - U_p''(t-2\tau_a) = &-\frac{EAc_a}{M_b}\big(U_p'(t) + U_p'(t-2\tau_a)\big)\\ &+ \frac{\epsilon a \zeta}{M_b}\big(-d_p(t) + d_p(t-2\tau_a)\big)\\ &+ \frac{2EAc_a}{M_b}V_p(t-\tau_a).\end{aligned} \tag{27b}$$

After linearization of (12) and (13) (for more details in derivation, refer to [52]), the perturbed depth-of-cut can be written as follows:

$$d_p(t) = n\left(U_p(t) - U_p(t-\tau_0) - \frac{V_0}{\Omega_0}\left(\Phi_p(t) - \Phi_p(t-\tau_0)\right)\right) \tag{28a}$$
$$\tau_0 = \frac{2\pi}{n\Omega_0}. \tag{28b}$$

B. Dimensionless Equations of Motion

Next, we will formulate a simpler, lower-dimensional, and more elegant dimensionless form of the equations of motion as a basis for control. By employing the following characteristic time and length scales:

$$t_* = \frac{J_b}{GJc_t}, \quad L_* = \frac{2J_b}{nt_*^2\epsilon a^2}. \tag{29}$$

The following dimensionless perturbed angular and axial displacements and the dimensionless perturbed angular and axial top-driven velocities are introduced as follows:

$$\phi := \Phi_p, \quad s := \frac{U_p}{L_*} \tag{30a}$$
$$\omega(\hat{t}) := \frac{2GJc_t}{J_b}t_*^2\Omega_p(t), \quad v(\hat{t}) := \frac{2EAc_a}{M_b}\frac{t_*^2}{L_*}V_p(t) \tag{30b}$$

where $\hat{t} := (t/t_*)$ is the dimensionless time, $\omega(\hat{t})$ is the dimensionless angular velocity of the top drive, which is considered as the torsional control input, and $v(\hat{t})$ is the dimensionless axial velocity of the top drive, which is considered as the axial control input. Eventually, the dimensionless form of (27) is obtained as follows:

$$\begin{aligned}\ddot{\phi}(\hat{t}) - \ddot{\phi}(\hat{t}-2\hat{\tau}_t) = &-\dot{\phi}(\hat{t}) - \dot{\phi}(\hat{t}-2\hat{\tau}_t)\\ &- \hat{d}(\hat{t}) + \hat{d}(\hat{t}-2\hat{\tau}_t) + \omega(\hat{t}-\hat{\tau}_t)\end{aligned} \tag{31a}$$

$$\ddot{s}(\hat{t}) - \ddot{s}(\hat{t} - 2\hat{\tau}_a) = -\kappa\dot{s}(\hat{t}) - \kappa\dot{s}(\hat{t} - 2\hat{\tau}_a) - \psi\hat{d}(\hat{t}) + \psi\hat{d}(\hat{t} - 2\hat{\tau}_a) + v(\hat{t} - \hat{\tau}_a) \tag{31b}$$

with the dot notation $\dot{()}$ denoting the differentiation with respect to the dimensionless time $\hat{t}$, and by introducing the following dimensionless parameters:

$$\chi = \frac{nV_0\epsilon a^2}{2J_b\Omega_0}t_*^2, \quad \kappa = \frac{EAc_a}{M_b}t_*, \quad \psi = \frac{n\epsilon a\zeta}{M_b}t_*^2 \tag{32a}$$

$$\hat{\tau}_t = \frac{\tau_t}{t_*}, \quad \hat{\tau}_a = \frac{\tau_a}{t_*}, \quad \hat{\tau}_0 = \frac{\tau_0}{t_*}. \tag{32b}$$

In addition,

$$\hat{d}(\hat{t}) := \frac{d_p(t)}{nL_*} = \big(s(\hat{t}) - s(\hat{t} - \hat{\tau}_0)\big) - \chi\big(\phi(\hat{t}) - \phi(\hat{t} - \hat{\tau}_0)\big) = \int_{\hat{t}-\hat{\tau}_0}^{\hat{t}} \big(\dot{s}(\theta) - \chi\dot{\phi}(\theta)\big)d\theta \tag{33}$$

is the dimensionless perturbed depth-of-cut. By choosing the dimensionless angular and axial velocities and the dimensionless depth-of-cut as the representative states, and recalling the dimensionless perturbed control inputs ω and v, the dimensionless dynamics (31) is expressed in the following third-order state-space form:

$$\dot{\bar{x}}_1(\hat{t}) - \dot{\bar{x}}_1(\hat{t} - 2\hat{\tau}_t) = -\bar{x}_1(\hat{t}) - \bar{x}_1(\hat{t} - 2\hat{\tau}_t) - \bar{x}_3(\hat{t}) + \bar{x}_3(\hat{t} - 2\hat{\tau}_t) + u_1(\hat{t} - \hat{\tau}_t) \tag{34a}$$

$$\dot{\bar{x}}_2(\hat{t}) - \dot{\bar{x}}_2(\hat{t} - 2\hat{\tau}_a) = -\kappa\bar{x}_2(\hat{t}) - \kappa\bar{x}_2(\hat{t} - 2\hat{\tau}_a) - \psi\bar{x}_3(\hat{t}) + \psi\bar{x}_3(\hat{t} - 2\hat{\tau}_a) + u_2(\hat{t} - \hat{\tau}_a) \tag{34b}$$

$$\bar{x}_3 = \int_{\hat{t}-\hat{\tau}_0}^{\hat{t}} \big(-\chi\bar{x}_1(\theta) + \bar{x}_2(\theta)\big)d\theta \tag{34c}$$

with the state vector

$$\bar{x}(\hat{t}) = \begin{bmatrix} \bar{x}_1(\hat{t}) \\ \bar{x}_2(\hat{t}) \\ \bar{x}_3(\hat{t}) \end{bmatrix} := \begin{bmatrix} \dot{\phi}(\hat{t}) \\ \dot{s}(\hat{t}) \\ \hat{d}(\hat{t}) \end{bmatrix} \tag{35}$$

and the inputs

$$u_1(\hat{t}) = \omega(\hat{t}), \quad u_2(\hat{t}) = v(\hat{t}). \tag{36}$$

Remark 1: Note that earlier NTD models of coupled-axial drill-string models were of fourth order. Recognizing that the axial and torsional displacements do not appear in the equations of motion independently, and the depth-of-cut is the only relevant position-level variable, has led to the lower-dimensional formulation of the dynamics in (34).

III. Controller Design

We consider the control problem of stabilizing the origin of the dynamics in (34), which implies the (local) stabilization of the constant angular velocity Ω_0 and the constant axial velocity V_0 for the original dynamics (which reflects the desired nominal drilling condition).

A. Challenges in Controller Design

The presence of input delays, state delays, and neutral-type delay terms in the drill-string system dynamics makes the control design challenging. The output variables needed in the (feedback) controller design can only be measured by the sensors (which are installed at the top of the drill string) in a delayed fashion due to the signal transmission time. A predictor is designed in Section IV dealing with input delays and limitations in sensing. The neutral terms in (9) introduce vertical asymptotes to the spectrum of the system. Since a state-feedback controller does not affect the neutral terms, such asymptotes are unchangeable and placing all poles of system (9)–(13) to the left of an arbitrary vertical margin in the complex plane is not possible by employing only a state-feedback control law. Furthermore, if the system is not formally stable, i.e., at least one of the asymptotes is located in the right-half complex plane or on the imaginary axis, the system is not stabilizable by applying only a state-feedback controller [56]. The neutral time delay in (9a), $2\tau_t$, is the time required for the torsional waves to have a round trip from the bit to the top of the drill string. This indicates a correlation between the neutral term, with $2\tau_t$ delay, and the wave reflection at the top side of the drill string. Such correlation also holds for the axial dynamics (9b). Based on this observation, the neutral terms are removed from the equations of motion by designing a precompensator in Section III-B. Next, the control inputs in the compensated coordinates are designed to exponentially stabilize the drill-string dynamics. To this end, a sufficient stability condition is presented in Section III-C used to support the feedback design.

B. Compensator Design Methodology

The neutral terms are compensated for in the equations of motion (9a) and (9b) by introducing the following input transformation:

$$\Omega(t) = \Omega_t(t) + \Omega_c(t) + \Omega_0, \quad \Omega_c(t) = \eta_t'(t) \tag{37a}$$

$$V(t) = V_t(t) + V_c(t) + V_0, \quad V_c(t) = \eta_a'(t) \tag{37b}$$

where $\Omega_t(t)$ and $V_t(t)$ are the transformed control inputs and $\Omega_c(t)$ and $V_c(t)$ are the compensation terms which are equal to $\eta_t'(t)$ and $\eta_a'(t)$ (with $\eta_t(t)$ and $\eta_a(t)$ defined in (3) as the up-traveling waves), respectively. Note that such input transformation is practically implementable since the values of $\eta_t'(t)$ and $\eta_a'(t)$ can be expressed in terms of the measurable top-side velocities and strains (measured by installing velocity and strain sensors right below the top drive) by multiplying (4b) and (5b) by $(1/c_t)$ and $(1/c_a)$, respectively, and adding those to (4a) and (5a) as follows:

$$\eta_t'(t) = \frac{1}{2}\frac{\partial\Phi}{\partial t}(0,t) + \frac{1}{2c_t}\frac{\partial\Phi}{\partial x}(0,t) \tag{38a}$$

$$\eta_a'(t) = \frac{1}{2}\frac{\partial U}{\partial t}(0,t) + \frac{1}{2c_a}\frac{\partial U}{\partial x}(0,t). \tag{38b}$$

On the other hand, by solving (4c), (4d), (5c), and (5d), $\eta_t'(t)$ and $\eta_a'(t)$ are given by

$$\eta_t'(t+\tau_t) = \frac{1}{2}\left(\frac{\partial\Phi}{\partial t}(L,t) + \frac{1}{c_t}\frac{\partial\Phi}{\partial x}(L,t)\right) \tag{39a}$$

$$\eta_a'(t+\tau_a) = \frac{1}{2}\left(\frac{\partial U}{\partial t}(L,t) + \frac{1}{c_a}\frac{\partial U}{\partial x}(L,t)\right). \tag{39b}$$

From (7a), $(\partial\Phi/\partial x)(L,t)$ can be written in terms of the bit angular acceleration $\Phi_b''(t)$ and the TOB, $T(t)$, as follows:

$$\frac{\partial \Phi}{\partial x}(L,t) = -\frac{1}{GJ}\big(J_b\Phi_b''(t) + T(t)\big) \tag{40}$$

and from (7b), $(\partial U/\partial x)(L,t)$ can be written in terms of the bit axial acceleration $U_b''(t)$ and the WOB, $W(t)$, as follows:

$$\frac{\partial U}{\partial x}(L,t) = -\frac{1}{EA}\big(M_b U_b''(t) + W(t)\big). \tag{41}$$

Substituting $(\partial\Phi/\partial x)(L,t)$ from (40) into (39a) and $(\partial U/\partial x)(L,t)$ from (41) into (39b) regarding $\Phi(L,t) = \Phi_b(t)$ and $U(L,t) = U_b(t)$, and then shifting the time, yields

$$\begin{aligned}\eta_t'(t) = &-\frac{J_b}{2GJc_t}\Phi_b''(t-\tau_t) + \frac{1}{2}\Phi_b'(t-\tau_t)\\ &-\frac{1}{2GJc_t}T(t-\tau_t)\end{aligned} \tag{42a}$$

$$\begin{aligned}\eta_a'(t) = &-\frac{M_b}{2EAc_a}U_b''(t-\tau_a) + \frac{1}{2}U_b'(t-\tau_a)\\ &-\frac{1}{2EAc_a}W(t-\tau_a).\end{aligned} \tag{42b}$$

Eventually, the system dynamics (9) is transformed by input transformation (37), with regards to (42), as follows:

$$\Phi_b''(t) = -\frac{GJc_t}{J_b}\Phi_b'(t) - \frac{1}{J_b}T(t) + \frac{2GJc_t}{J_b}\Omega_t(t-\tau_t) \tag{43a}$$

$$U_b''(t) = -\frac{EAc_a}{M_b}U_b'(t) - \frac{1}{M_b}W(t) + \frac{2EAc_a}{M_b}V_t(t-\tau_a). \tag{43b}$$

Compared with (9a) and (9b), the transformed system (43a) and (43b) does not include any neutral term, and hence, their spectrum does not have any vertical asymptotes. Moreover, some other delayed terms of (9a) and (9b) disappeared in (43a) and (43b). Subsequently, the dimensionless form of the transformed dynamics (43a) and (43b), after linearization around the steady-state solution (according to the procedure in Sections II-B and II-A) is obtained as follows:

$$\ddot{\phi}(\hat{t}) = -\dot{\phi}(\hat{t}) - \hat{d}(\hat{t}) + \omega_t(\hat{t}-\hat{\tau}_t) \tag{44a}$$

$$\ddot{s}(\hat{t}) = -\kappa\dot{s}(\hat{t}) - \psi\hat{d}(\hat{t}) + v_t(\hat{t}-\hat{\tau}_a) \tag{44b}$$

where $\omega_t(\hat{t})$ and $v_t(\hat{t})$ represent the dimensionless perturbed form of the transformed control inputs $\Omega_t(t)$ and $V_t(t)$ in (37), respectively. Note that the dimensionless form of the control inputs (before applying the compensator) (37) is given as follows:

$$\omega(\hat{t}) = \omega_t(\hat{t}) + \omega_c(\hat{t}) \tag{45a}$$

$$v(\hat{t}) = v_t(\hat{t}) + v_c(\hat{t}) \tag{45b}$$

where

$$\omega_c(\hat{t}) = \ddot{\phi}(\hat{t}-2\hat{\tau}_t) - \dot{\phi}(\hat{t}-2\hat{\tau}_t) + \hat{d}(\hat{t}-2\hat{\tau}_t) \tag{46a}$$

$$v_c(\hat{t}) = \ddot{s}(\hat{t}-2\hat{\tau}_a) - \kappa\dot{s}(\hat{t}-2\hat{\tau}_a) + \psi\hat{d}(\hat{t}-2\hat{\tau}_a) \tag{46b}$$

are the dimensionless compensation terms formulated in terms of down-hole variables. In order to standardize the notation, the following notation for the components of the control inputs, $u_{1_c}(\hat{t})$, $u_{1_t}(\hat{t})$, $u_{2_c}(\hat{t})$, and $u_{2_t}(\hat{t})$ are introduced:

$$u_{1_c}(\hat{t}) := \omega_c(\hat{t}), \quad u_{1_t}(\hat{t}) := \omega_t(\hat{t}) \tag{47a}$$

$$u_{2_c}(\hat{t}) := v_c(\hat{t}), \quad u_{2_t}(\hat{t}) := v_t(\hat{t}). \tag{47b}$$

Employing (35) as a representative state vector for (44), regarding (47), yields the following third-order state-space formulation of the dynamics after applying the precompensator:

$$\dot{\bar{x}}_1(\hat{t}) = -\bar{x}_1(\hat{t}) - \bar{x}_3(\hat{t}) + u_{1_t}(\hat{t}-\hat{\tau}_t) \tag{48a}$$

$$\dot{\bar{x}}_2(\hat{t}) = -\kappa\bar{x}_2(\hat{t}) - \psi\bar{x}_3(\hat{t}) + u_{2_t}(\hat{t}-\hat{\tau}_a) \tag{48b}$$

$$\bar{x}_3(\hat{t}) = \int_{\hat{t}-\hat{\tau}_0}^{\hat{t}} \big(-\chi\bar{x}_1(\theta) + \bar{x}_2(\theta)\big)d\theta. \tag{48c}$$

As a consequence, the proposed precompensation strategy simplifies the dynamics to be stabilized, allowing the stabilizing controller design discussed in Section III-C to be implementable.

C. State-Feedback Control Design Methodology

The following state-feedback control law is defined:

$$u_{1_t}(\hat{t}) = -K_1 x(\hat{t}+\hat{\tau}_t) \tag{49a}$$

$$u_{2_t}(\hat{t}) = -K_2 x(\hat{t}+\hat{\tau}_a) \tag{49b}$$

which is noncausal and cannot be directly implemented. To make the control law causal, a predictor will be designed in Section IV. The following structure is proposed for the gain matrices in (49):

$$K_1 = \begin{bmatrix}k_{11} & 0 & k_{13}\end{bmatrix}, \quad K_2 = \begin{bmatrix}0 & k_{22} & k_{23}\end{bmatrix} \tag{50}$$

with the scalars k_{11}, k_{13}, k_{22}, and k_{23}, as the controller gains. These gains are designed aiming at placing all poles of the system (48) in the left-half-plane $R_{-\nu}^{-} = \{\lambda|\mathrm{Re}(\lambda) \le -\nu\}$ for an arbitrary, strictly positive value ν, which itself is a design parameter. The structure in (50) is proposed as, intuitively, it seems that the torsional dynamics can be stabilized by applying a linear combination of the bit angular velocity and the TOB (which is itself proportional to the depth-of-cut) as the control torque. Moreover, the axial dynamics may be stabilized by applying a linear combination of the axial velocity and the WOB (which also depends on the depth-of-cut). Furthermore, considering two entries in the gain matrices equal to zero alleviates the computational burden of the controller design. The closed-loop dynamics is obtained by substituting (49) into (48) as follows:

$$\dot{\bar{x}}_1(\hat{t}) = (k_{11}-1)\bar{x}_1(\hat{t}) + (k_{13}-1)\bar{x}_3(\hat{t}) \tag{51a}$$

$$\dot{\bar{x}}_2(\hat{t}) = (k_{22}-\kappa)\bar{x}_2(\hat{t}) + (k_{23}-\psi)\bar{x}_3(\hat{t}) \tag{51b}$$

$$\bar{x}_3(\hat{t}) = \int_{\hat{t}-\hat{\tau}_0}^{\hat{t}} \big(-\chi\bar{x}_1(\theta) + \bar{x}_2(\theta)\big)d\theta. \tag{51c}$$

Subsequently, the characteristic matrix of the closed-loop system (51) is given by

$$\Delta_c(\lambda) = \begin{bmatrix} \lambda + 1 - k_{11} & 0 & 1 - k_{13} \\ 0 & \lambda + \kappa - k_{22} & \psi - k_{23} \\ \chi g(\lambda) & -g(\lambda) & 1 \end{bmatrix} \quad (52)$$

where

$$g(\lambda) = \frac{1 - e^{-\hat{\tau}_0 \lambda}}{\lambda}. \quad (53)$$

In the following theorem, we provide analytical synthesis conditions in terms of the system parameters, κ, ψ, and χ, defined in (32), that ensure the stabilization of the closed-loop dynamics (51) with guaranteed exponential convergence rate.

Theorem 1: If the following relations exist between the control gains and the system parameters (51):

$$1 - k_{11} > \nu, \quad \kappa - k_{22} > \nu \quad (54a)$$

$$1 - k_{13} > 0, \quad \psi - k_{23} > 0 \quad (54b)$$

$$\frac{1 + e^{\tau_0 \nu}}{\nu} \left(\frac{\chi(1 - k_{13})}{1 - k_{11} - \nu} + \frac{\psi - k_{23}}{\kappa - k_{22} - \nu} \right) \leq 1 \quad (54c)$$

then all poles of the closed-loop system (51) are located in the half-plane $R^-_{-\nu} = \{\lambda | \mathrm{Re}(\lambda) \leq -\nu\}$.

Proof: Assume that there exists an undesirable characteristic root λ_r belonging to the complex set $R^+_{-\nu} = \{x | \mathrm{Re}(x) > -\nu\}$ that vanishes the determinant of the characteristic matrix (52). Correspondingly, there exists a nontrivial normalized eigenvector

$$V_r = \frac{1}{\sqrt{v_1^2 + v_2^2 + v_3^2}} \begin{bmatrix} v_1 \\ v_2 \\ v_3 \end{bmatrix} \quad (55)$$

which belongs to the null space of the characteristic matrix (52) for $\lambda = \lambda_r$ by satisfying the following equation:

$$\begin{bmatrix} \lambda_r + 1 - k_{11} & 0 & 1 - k_{13} \\ 0 & \lambda_r + \kappa - k_{22} & \psi - k_{23} \\ \chi g(\lambda_r) & -g(\lambda_r) & 1 \end{bmatrix} \begin{bmatrix} v_1 \\ v_2 \\ v_3 \end{bmatrix} = 0. \quad (56)$$

This matrix equation can be rewritten as three complex equations as follows:

$$(\lambda_r + 1 - k_{11}) v_1 = -(1 - k_{13}) v_3 \quad (57a)$$

$$(\lambda_r + \kappa - k_{22}) v_2 = -(\psi - k_{23}) v_3 \quad (57b)$$

$$\chi g(\lambda_r) v_1 - g(\lambda_r) v_2 = -v_3 \quad (57c)$$

which gives the following magnitude equalities:

$$|\lambda_r + 1 - k_{11}||v_1| = |1 - k_{13}||v_3| \quad (58a)$$

$$|\lambda_r + \kappa - k_{22}||v_2| = |\psi - k_{23}||v_3| \quad (58b)$$

$$|g(\lambda_r)||\chi v_1 - v_2| = |v_3|. \quad (58c)$$

The following inequality can be obtained from (58c) according to Lemma 2 in Appendix and the triangle inequality:

$$|v_3| \leq |g(\lambda_r)|(\chi |v_1| + |v_2|) \leq \frac{1 + e^{-\hat{\tau}_0 \nu}}{\nu} (\chi |v_1| + |v_2|). \quad (59)$$

Moreover, regarding Lemma 1 in Appendix and condition (54b), the following inequalities can be obtained:

$$|\lambda_r + 1 - k_{11}| > 1 - k_{11} - \nu \quad (60a)$$

$$|\lambda_r + 1 - k_{22}| > 1 - k_{22} - \nu. \quad (60b)$$

Substituting (60) in (58a) and (58b) gives the following inequalities with regards to (54b):

$$|v_1| < \frac{1 - k_{13}}{1 - k_{11} - \nu} |v_3| \quad (61a)$$

$$|v_2| < \frac{\psi - k_{23}}{\kappa - k_{22} - \nu} |v_3|. \quad (61b)$$

Substituting (61) into (59) gives

$$|v_3| < \frac{1 + e^{-\hat{\tau}_0 \nu}}{\nu} \left(\frac{\chi(1 - k_{13})}{1 - k_{11} - \nu} + \frac{\psi - k_{23}}{\kappa - k_{22} - \nu} \right) |v_3| \quad (62)$$

resulting in the following relation:

$$\frac{1 + e^{-\hat{\tau}_0 \nu}}{\nu} \left(\frac{\chi(1 - k_{13})}{1 - k_{11} - \nu} + \frac{\psi - k_{23}}{\kappa - k_{22} - \nu} \right) > 1 \quad (63)$$

which is in contradiction with the condition (54c). Consequently, the assumption in the first sentence of the proof is incorrect, and the theorem is proved by contradiction. □

Theorem 1 already establishes synthesis conditions for the feedback controller gains (parameterized by the drill-string system parameters). However, the controller gains cannot be obtained explicitly from the relations in Theorem 1. Now, in Proposition 1, the controller gains are explicitly stated in terms of the drill-string system parameters based on the conditions presented in Theorem 1.

Proposition 1: Let arbitrary, positive real numbers, d_1–d_4, satisfy the following equation:

$$1 - d_3 - d_4 > 0. \quad (64)$$

Then, the following control gains guarantee that all poles of the closed-loop system (51) are located in the left-half complex plane $R^-_{-\nu} = \{\lambda | \mathrm{Re}(\lambda) \leq -\nu\}$:

$$k_{11} = 1 - \nu - d_1, \quad k_{22} = \kappa - \nu - d_2$$
$$k_{13} = 1 - \frac{d_1 d_3}{\chi \frac{1 + e^{-\hat{\tau}_0 \nu}}{\nu}}, \quad k_{23} = \psi - \frac{d_2}{\frac{1 + e^{-\hat{\tau}_0 \nu}}{\nu}} (1 - d_3 - d_4). \quad (65)$$

Proof: Since d_1–d_3, and $1 - d_3 - d_4$ are all positive values, the first condition of Theorem 1, (54b), is satisfied. The following relation arises directly from (65):

$$\frac{1 + e^{\tau_0 \nu}}{\nu} \left(\frac{\chi(1 - k_{13})}{1 - k_{11} - \nu} + \frac{\psi - k_{23}}{\kappa - k_{22} - \nu} \right) = 1 - d_4. \quad (66)$$

Since d_4 is a positive value, the following inequality holds:

$$1 - d_4 < 1. \quad (67)$$

Hence, the second condition of the theorem, (54c), is satisfied as well and the statement is proved according to Theorem 1. □

Remark 2: Compared to the existing approaches for NDDE models, the novel control design method is applicable for different drill-string systems, without the need for redesigning the controller because it explicitly gives the control gains as a function of the drill-string parameters. Moreover, the exponential decay rate of the closed-loop dynamics is one of the design parameters with the aid of the precompensator.

IV. Predictor Design Methodology

The state-feedback controller (49) is noncausal since it requires future state values. To make such a controller causal, a predictor is proposed in this section to predict future states based on the available measurements. An implementable predictor for systems with state delays and several input delays is developed in [43]. In order to use such a predictor, we rewrite system (48) in the form of the system class considered in [43], with regards to the available measurements.

In this article, it is assumed that only angular and axial velocity sensors [measuring $(\partial\Phi/\partial t)(0,t)$ and $(\partial U/\partial t)(0,t)$] and saver subtorque and force sensors [measuring $(\partial\Phi/\partial x)(0,t)$ and $(\partial U/\partial x)(0,t)$] are installed at the top side of the string, right below the top drive. Subsequently, $(\partial\Phi_b/\partial t)(t-\tau_t)$ and $(\partial U_b/\partial t)(t-\tau_a)$ are available (indirectly) by solving (4) and (5) as follows [52]:

$$\frac{\partial\Phi_b}{\partial t}(t-\tau_t)=\frac{1}{2}\left(\frac{\partial\Phi}{\partial t}(0,t)+\frac{1}{c_t}\frac{\partial\Phi}{\partial x}(0,t)+\frac{\partial\Phi}{\partial t}(0,t-2\tau_t)-\frac{1}{c_t}\frac{\partial\Phi}{\partial x}(0,t-2\tau_t)\right) \tag{68a}$$

$$\frac{\partial U_b}{\partial t}(t-\tau_a)=\frac{1}{2}\left(\frac{\partial U}{\partial t}(0,t)+\frac{1}{c_a}\frac{\partial U}{\partial x}(0,t)+\frac{\partial U}{\partial t}(0,t-2\tau_a)-\frac{1}{c_a}\frac{\partial U}{\partial x}(0,t-2\tau_a)\right). \tag{68b}$$

Since the shear modulus of the drill pipes is less than its elastic modulus, the torsional wave has a lower speed than the axial wave, i.e., $\tau_t>\tau_a$. Accordingly, all states of (48) are available at $\hat{t}-\hat{\tau}_t$, i.e., $\bar{x}_1$ and $\bar{x}_2$ are available directly and $\bar{x}_3$ is obtained by integrating $\bar{x}_1$ and $\bar{x}_2$ from $\hat{t}-\hat{\tau}_t-\hat{\tau}_0$ to $\hat{t}-\hat{\tau}_t$.

An alternative representation of $\bar{x}_3(\hat{t})$ in (48) is formulated by differentiating (51c) and specifying the initial value for $\bar{x}_3$ as a function of the initial values of $\bar{x}_1$ and $\bar{x}_2$ as follows:

$$\dot{\bar{x}}_3(\hat{t})=-\chi\bar{x}_1(\hat{t})+\chi\bar{x}_1(\hat{t}-\hat{\tau}_t)+\bar{x}_2(\hat{t})-\bar{x}_2(\hat{t}-\hat{\tau}_t) \tag{69a}$$

$$\bar{x}_3(0)=\int_{-\hat{\tau}_0}^{0}\big(-\chi\bar{x}_1(\theta)+\bar{x}_2(\theta)\big)d\theta. \tag{69b}$$

Accordingly, (48) can be reformulated as follows:

$$\dot{\bar{x}}(\hat{t})=A_0\bar{x}(\hat{t})+A_1\bar{x}(\hat{t}-\hat{\tau}_0)+B_1u_{1_t}(\hat{t}-\hat{\tau}_t)+B_2u_{2_t}(\hat{t}-\hat{\tau}_a) \tag{70a}$$

$$\bar{x}_3(0)=\int_{-\hat{\tau}_0}^{0}\big(-\chi\bar{x}_1(\theta)+\bar{x}_2(\theta)\big)d\theta \tag{70b}$$

$$y(\hat{t})=\bar{x}(\hat{t}-\hat{\tau}_t) \tag{70c}$$

where

$$A_0=\begin{bmatrix}-1&0&-1\\0&-\kappa&-\psi\\-\chi&1&0\end{bmatrix},\quad A_1=\begin{bmatrix}0&0&0\\0&0&0\\\chi&-1&0\end{bmatrix} \tag{71a}$$

$$B_1=\begin{bmatrix}1\\0\\0\end{bmatrix},\quad B_2=\begin{bmatrix}0\\1\\0\end{bmatrix} \tag{71b}$$

and $y(\hat{t})$ is the available, measured output. By defining the following new state vector by shifting the time

$$x(\hat{t})=\bar{x}(\hat{t}-\hat{\tau}_t). \tag{72}$$

The measurement delay in (70) is added to the input delay as follows:

$$\dot{x}(\hat{t})=A_0x(\hat{t})+A_1x(\hat{t}-\hat{\tau}_0)+B_1u_{1_t}(\hat{t}-2\hat{\tau}_t)+B_2u_{2_t}(\hat{t}-\hat{\tau}_t-\hat{\tau}_a) \tag{73a}$$

$$x_3(0)=\int_{-\hat{\tau}_0}^{0}\big(-\chi x_1(\theta)+x_2(\theta)\big)d\theta \tag{73b}$$

$$y=x(\hat{t}). \tag{73c}$$

Now in (73), all states at $\hat{t}$ are available and the approach proposed in [43] can be employed to design a predictor for (73).

The predictor-based controller law is defined as follows:

$$\begin{aligned}u_{2_{td}}(\hat{t})=&\,Q_v(\hat{\tau}_a+\hat{\tau}_t)x(\hat{t})\\&+\int_{-\hat{\tau}_0}^{0}Q_v(\hat{\tau}_a+\hat{\tau}_t-\hat{\tau}_0-\theta)A_1x(\hat{t}+\theta)d\theta\\&+\int_{-\hat{\tau}_a-\hat{\tau}_t}^{0}Q_v(-\theta)B_2u_{2_{td}}(\hat{t}+\theta)d\theta\\&+\int_{-2\hat{\tau}_t}^{\hat{\tau}_a-\hat{\tau}_t}Q_v(\hat{\tau}_a-\hat{\tau}_t-\theta)B_1u_{1_{td}}(\hat{t}+\theta)d\theta\end{aligned} \tag{74a}$$

$$\begin{aligned}u_{1_{td}}(\hat{t})=&\,Q_\omega(\hat{\tau}_t-\hat{\tau}_a)x(\hat{t})\\&+\int_{-\hat{\tau}_0}^{0}Q_v(\hat{\tau}_t-\hat{\tau}_a-\hat{\tau}_0-\theta)A_1x(\hat{t}+\theta)d\theta\\&+\int_{-\hat{\tau}_a-\hat{\tau}_t}^{0}Q_\omega(-\theta)B_1u_{2_{td}}(\hat{t}+\theta)d\theta\\&+\int_{-2\hat{\tau}_t}^{\hat{\tau}_a-\hat{\tau}_t}Q_\omega(\hat{\tau}_a-\hat{\tau}_t-\theta)B_1\omega(\hat{t}+\theta)d\theta\\&+\int_{\hat{\tau}_a-\hat{\tau}_t}^{0}\big(K_2K^{**}(-\theta)\big)B_1\omega(\hat{t}+\theta)d\theta\end{aligned} \tag{74b}$$

where $u_{2_{td}}$ and $u_{1_{td}}$ are the desired (and unfiltered) causal alternatives for the noncausal control inputs, u_{2_t} and u_{1_t}, in (49) with Q_v, Q_ω, K_2, and K^{**} given in Appendix.

Theorem 2: By employing the control law (74a) and (74b), eigenvalues of (73) are equal to the eigenvalues of the following equation:

$$\dot{x}(\hat{t})=(A_0+B_1K_1+B_2K_2)x(\hat{t})+A_1x(\hat{t}-\hat{\tau}_0). \tag{75}$$

Proof: This theorem is proved in [43]. □

Note that the (precompensated) dynamics (48) with the noncausal control law (49) is equivalent with the system (75). Hence, Theorem 2 illustrates that applying the causal control law (74) to the dynamics (48) is equivalent with applying the noncausal control law (49), in the sense of the system spectrum. According to Proposition 1, employing the designed control gains (65) makes system (48) with the noncausal control law (49) exponentially stable. Consequently, regarding Proposition 1, employing the designed control gains (65) together with the causal control law (74) make the system (48) exponentially stable. As a conclusion, the control design approach presented in Section III and the predictor-based law (74) together exponentially stabilize the closed-loop system.

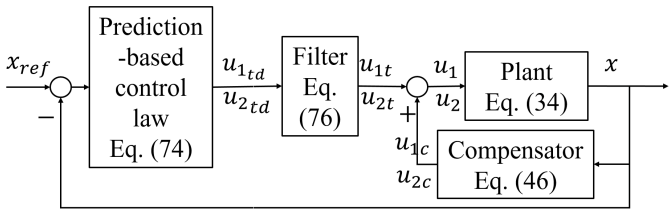

Fig. 2. Total closed-loop block diagram.

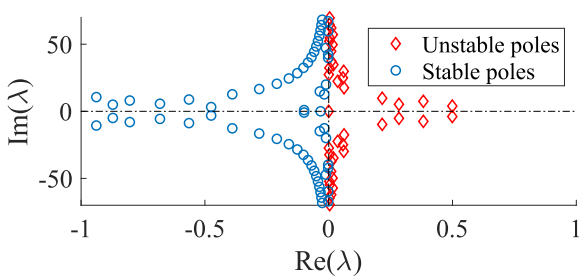

Fig. 3. Open-loop spectrum.

A. Implementation Aspects

Finite integral sums should be used to approximate integrals in (74a) and (74b) in simulations. When the equations are not internally stable, this leads to closed-loop system instability for systems with input delays [39], [40], and [41]. By observing the frequency behavior of the unstable dynamics, adding a low-pass filter was proposed in [42]. Based on this idea, the prediction-based parts of the control inputs are filtered as follows:

$$(\dot{u}_{1_t}(\hat{t}) - \dot{u}_{1_{td}}(\hat{t})) = -\vartheta_t(u_{1_t}(\hat{t}) - u_{1_{td}}(\hat{t})) \tag{76a}$$

$$(\dot{u}_{2_t}(\hat{t}) - \dot{u}_{2_{td}}(\hat{t})) = -\vartheta_a(u_{2_t}(\hat{t}) - u_{2_{td}}(\hat{t})) \tag{76b}$$

where ϑ_t and ϑ_a are positive constants greater than ν, the arbitrary positive number defined in Section III for exponential stability.

The total control scheme composed of the compensator-based part (46), and predictor-based part (74), (76) is shown in Fig. 2.

V. Simulation Results

In this section, a representative case study is presented to illustrate the effectiveness of the proposed control law (37) and (49) for system (34). In Section V-A, the open-loop dynamics are analyzed, and in Section V-B, the controller performance and the resulting closed-loop behavior of the system are illustrated. The robustness of the proposed controller against parametric uncertainty and disturbance is investigated in Section V-C. Eventually, the controller, which was designed for the linearized system, is applied to the original nonlinear system and its effectiveness is examined in the fully nonlinear context. The parameter values used for simulations are given in Table I in the SI unit system.

A. Open-Loop Dynamics Analysis

The open-loop spectrum of the system (34) for $u_1(\hat{t}) = u_2(\hat{t}) = 0$ is shown in Fig. 3. The TDS-STABIL MATLAB package [59] is employed to find the stability-relevant characteristic roots of the system. The existence of some characteristic roots in the RHP indicates that the system is inherently unstable. The existence of unstable poles in the absence of the controller is due to the combination of the infinite-dimensional drill-string dynamics and the regenerative effect of the cutting process at the bit (which has been recognized in [13], [28], and [60]). Moreover, the vertical asymptote of the poles at the imaginary axis is due to the neutral nature of (34). The existence of such vertical asymptote has already been observed in [52]. The time evolution of the fully nonlinear system [the dynamics (9) with the nonlinear bit–rock interaction law (10)–(13)] with constant top-driven velocities $\Omega(t) = 4.71$ rad/s (45 r/min) and $V(t) = 0.0028$ m/s (5 m/h) is shown in Fig. 4. Fig. 4 illustrates that in the absence of control, unstable poles of the linearized dynamics lead to torsional and axial stick–slip oscillations in the nonlinear dynamics, which in practice may result in system failure or reduced drilling performance. These stick–slip limit cycles are induced by the set-valued nature of the axial and torsional bit–rock interaction laws in (11) [especially those related to the wear flat, see (11b) and (11d)]. For more details on the root causes of such stick–slip oscillations the reader may refer to [11], [13], [14], and [28]. These results are in agreement with previous studies [11], [13], [14], [15], [16], [60], which show that for realistic parameter values, the steady-state solution is generally unstable.

As explained in Section III, for formal stability, vertical asymptotes of the spectrum should be located in the left

TABLE I
Parameter Values [52]

Parameter	Definition	Value
Ω_0	Nominal angular velocity	45 rpm
V_0	Nominal axial velocity	10 m/h
M_b	BHA mass	40000 kg
J_b	BHA moment of inertia	89 kgm^2
E	Young modulus	200×10^9 N/m^2
G	Shear modulus	79×10^9 N/m^2
ρ	Density	8000 kg/m^3
A	drill-string cross sectional area	35×10^{-4} m^2
J	drill-string moment of area	1.9×10^{-5} m^4
L	drill-string length	1172 m
ε	Rock intrinsic specific energy	60×10^6 N/m^2
a	Bit radius	10.8×10^{-2} m
ζ	Cutter face inclination number	0.6
σ	Maximum constant pressure at the wearflat interface	60×10^6 N/m^2
l	Length of the drill bit wearflat	1.2×10^{-3} m
μ	Friction coefficient at the wearflat-rock interface	0.6
γ	Bit geometry number	1
n	number of blades	4

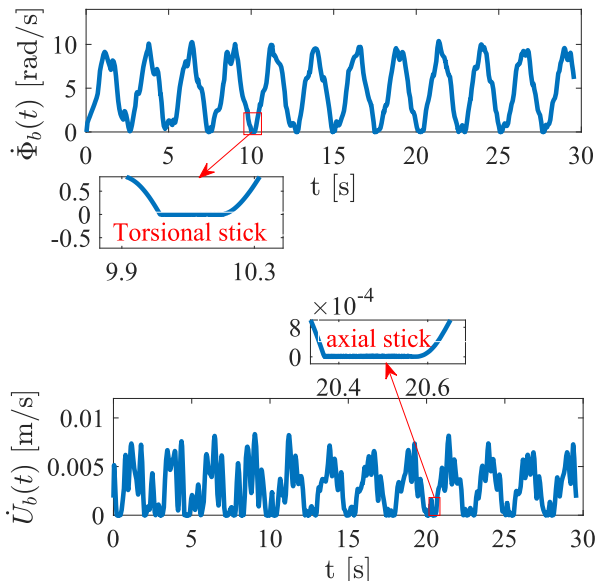

Fig. 4. Open-loop angular and axial velocity of the bit.

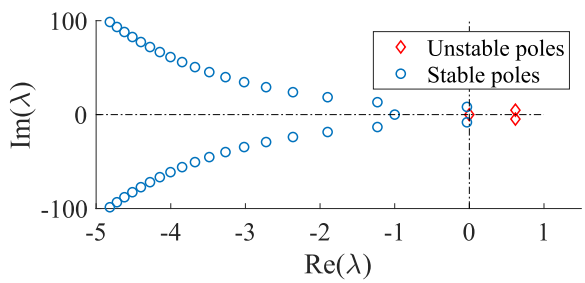

Fig. 5. Spectrum after applying the compensator.

half-plane. As shown in Fig. 3, the asymptote of the NTD system (34) is located on the imaginary axis and the roots are accumulated on the imaginary axis. Hence, the system is not formally stable and state feedback can not stabilize the system. This illustrates that the usage of the proposed compensator is indeed essential.

B. Closed-Loop Dynamics Analysis

The spectrum of the compensated system (48), with $u_{1_t} = u_{2_t} = 0$, is depicted in Fig. 5. Compared to Fig. 3, the number of unstable poles is decreased, and there is no root accumulation near the imaginary axis (the vertical asymptote observed in Fig. 3 disappeared in Fig. 5) since there is no neutral term in (43). However, there are still some unstable poles. As mentioned above, the interaction of the drill-string dynamics with the regenerative effect caused by the cutting process is the root cause of this instability and is still present after implementing the compensator. The effect of applying the compensator on the behavior of the nonlinear system, which is (43) with $\Omega_t = V_t = 0$ and the nonlinear bit–rock interaction law (10)–(13), is depicted in Fig. 6. In the first 10 s of operation, the system is operating with constant top-driven angular and axial velocities, as in Fig. 4. Then, at the time $t = 10$ s, the compensator is applied to the system, i.e., the

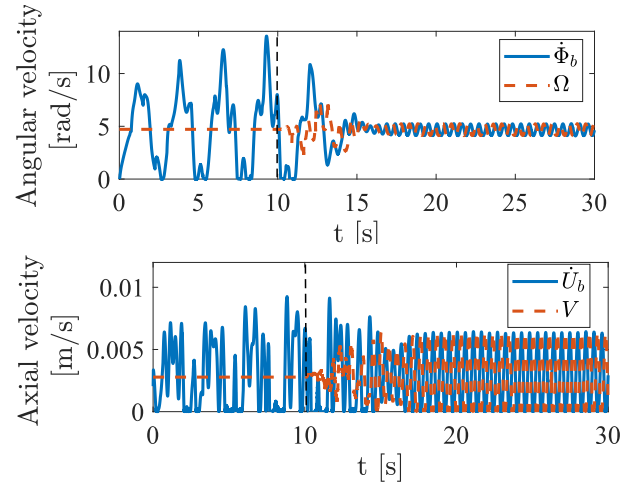

Fig. 6. Angular and axial velocity of the bit and the top drive in the presence of the compensator. The vertical dashed line indicates the time instant at which the compensator is turned on.

top-driven angular and axial velocities are governed by (37) with $\Omega_t(t) = V_t(t) = 0$. It is observed that applying the compensator mitigates torsional stick–slip and reduces the torsional oscillations significantly. However, axial stick–slip motions still occur.

To fully stabilize the dynamics and to mitigate all oscillations completely, the state-feedback law (49) is applied to the system, in addition to the compensator. Regarding (65) and (64), by choosing $d_1 = d_2 = 2$, $d_3 = 0.5$, $d_4 = 0.1$, and $\nu = 3$, the control gains are designed as follows to exponentially stabilize the system, i.e., to place all roots such that their real values are less than $-\nu = -3$:

$$k_{11} = -4, \quad k_{22} = -4.35, \; k_{13} = 0.72, \; k_{23} = -109.9. \tag{77}$$

Note that, although choosing greater values for ν decreases the settling time of the transient response, it demands larger control action in these transients (typically also with higher frequencies), making the controller impractical due to the physical restrictions of the top-driven actuator. Furthermore, further increasing the gain may detrimentally affect the sensitivity to disturbances and unmodeled dynamics. Numerical results show that for a drill string with parameter values presented in Table I, $\nu = 3$ provides a good balance in this respect. The spectrum of the closed-loop system is illustrated in Fig. 7. As can be seen, all roots have real values less than the intended value $-\nu = -3$, which guarantees the exponential stability of the closed-loop system with the desired decay rate. The vertical asymptotes of the spectrum are eliminated, and the feedback control could place all the characteristic roots on the left-hand side of the desired vertical line. The latter fact emphasizes the importance of compensator design presented in Section III.

The behavior of the linearized system after applying the compensator and the predictor-based controller (74) and the filter (76) is shown in Fig. 8 which shows that indeed the bit velocities converge to the desired constant velocities. The desired (reference) angular velocity is 4.71 rad/s (45 r/min) and

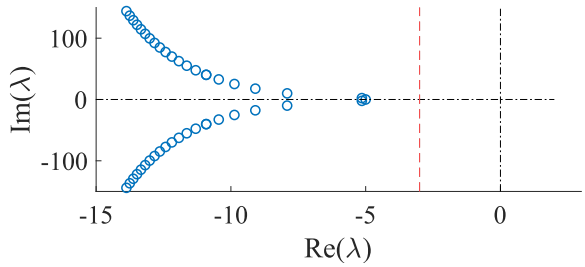

Fig. 7. Closed-loop spectrum of the system with compensator and state-feedback law (49). The red vertical line divides the complex plane into the desirable half-plane $R^{-}_{-\nu} = \{\lambda | \mathrm{Re}(\lambda) \leq -\nu\}$ and the undesirable half-plane $R^{+}_{-\nu} = \{\lambda | \mathrm{Re}(\lambda) > -\nu\}$ for $\nu = 3$.

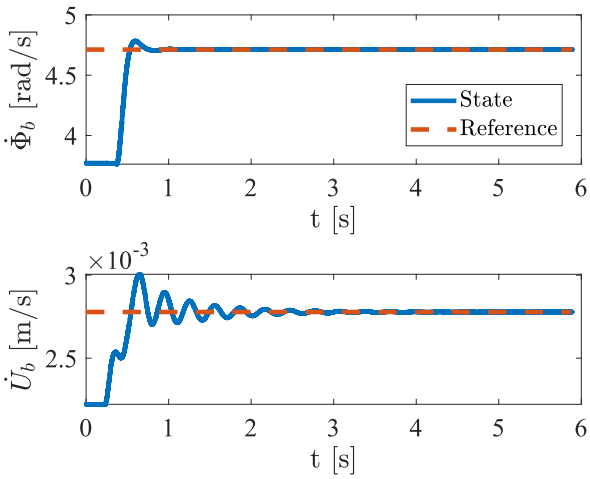

Fig. 8. Closed-loop behavior of the system.

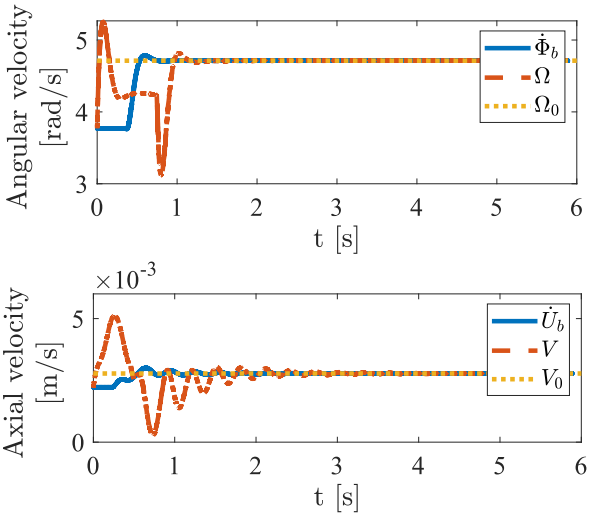

Fig. 9. Control inputs (top-side velocities) and bit velocities of the closed-loop system.

the desired (reference) axial velocity is 0.0028 m/s (10 m/h). Although the controller is activated at the time $t = 0$, the bit accelerates with a time delay. This is the time delay required for the torsional and axial waves to reach the bit, which is $\tau_t = 0.325$ s for the torsional dynamics and $\tau_a = 0.235$ s for the axial dynamics. The axial and torsional control inputs are depicted in Fig. 9.

In [52], the control problem is defined as a trajectory tracking problem. Namely, the controller in [52] introduces

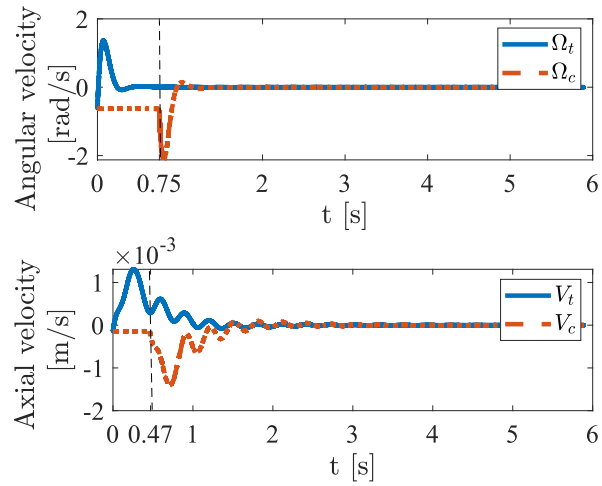

Fig. 10. Compensation and prediction-based components of the control inputs.

large overshoots and high-frequency content to the system response in the presence of (step-wise) references to constant angular and axial velocities. Therefore, a smoothened reference trajectory is employed to prevent such large overshoots. The controller proposed in this article does not have this drawback and can regulate the system state without introducing large overshoots and high-frequency responses in the control actions, even in the presence of (step-wise) constant references, which shows the practical implementability of the proposed controller. Fig. 9 shows that the effect of control actuation on the bit occurs with a delay, which is according to the input time delays in (9) induced by the distributed nature (wave propagation) of the drill-string model. The compensator- and predictor-based parts of the control inputs are shown in Fig. 10, separately. First, the prediction-based control action aims at increasing the bit velocities to the desired ones. When the associated waves reach the bit, the signature of such signals is reflected in accordance with the boundary condition associated with the bit–rock interaction and travels upward. Accordingly, the torsional and axial signals reach the top side after passing $2\tau_t = 0.75$ s and $2\tau_a = 0.47$ s, respectively. At this time, the compensator prevents the signals from traveling downward again since the bit velocities have approached the desired ones and the initial feedback action not be reflected downward again.

It should be noted that in this simulation analysis, white Gaussian noise is added to the measured outputs, with the signal-to-noise ratio (SNR) equal to 10. As a conclusion, the proposed controller and the predictor are robust against the measurement noise.

C. Analysis of Robustness Against Parametric Uncertainty

In drilling systems, the largest uncertainties are mostly associated with the parameters characterizing the bit–rock interaction [7], [52]. Therefore, the robustness of the designed controller is investigated in this section to evaluate the effectiveness of the controller in more realistic drilling conditions, i.e., conditions in which the rock parameters are not exactly known. The rock intrinsic specific energy ϵ and the cutter face

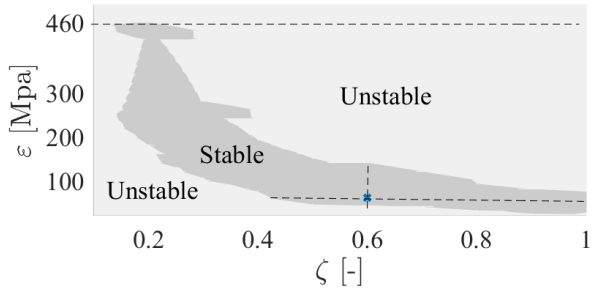

Fig. 11. Stable and unstable region in the presence of uncertainties in the bit–rock interaction parameters. The cross mark indicates the point for which the controller is designed.

inclination number ζ are considered uncertain for this purpose. In this scenario, the fixed controller, which is designed for the nominal values of the rock intrinsic specific energy $\epsilon = 60$ MPa and the face inclination number $\zeta = 0.6$ is applied to different formations with different actual values of ϵ and ζ. In Fig. 11, the $\zeta\epsilon$ plane is divided into the stable and unstable subregions based on the abscissa (i.e., the real part of the right-most eigenvalue) of the closed-loop system. In the $\zeta\epsilon$ plane, the point for which the controller is designed is marked with a cross. For a fixed value of ζ equal to the nominal value 0.6, the controller (which was designed for $\epsilon = 60$ MPa) is stabilizing for a range of (uncertain) ϵ between 45 and 137 MPa indicating the robustness of the controller in the presence of 25% uncertainty in ϵ. On the other hand, for a fixed value of ϵ equal to the nominal value 60 MPa, the controller (which was designed for $\zeta = 0.6$) is stabilizing for a range of (uncertain) ζ between 0.43 and 1 indicating the robustness of the controller in the presence of 28% uncertainty in ζ. Moreover, for the cases with uncertainties in both ϵ and ζ, it is observed that the abovementioned (fixed) controller stabilizes the closed-loop system for a (relatively) wide range of uncertainties in the bit–rock interaction parameters. By increasing ϵ, the interval for ζ in which the closed-loop system is stable becomes smaller, and finally, the system becomes unstable for any amount of ζ when $\epsilon > 460$ MPa, which is corresponding to a formation with extremely hard rock. In other words, the stability is weakening (to a limited extent) when the formation becomes harder, which is intuitive. It should be noted that outside these ranges, other controller tunings can be pursued to induce stability in the area that is now unstable.

D. Implementation of the Controller to the Nonlinear System

In this section, the effectiveness of the proposed controller when it is applied to the drilling dynamics (9) with the nonlinear bit–rock interaction (10)–(13) is investigated. This study is performed to assess the applicability of the proposed control strategy in the nonlinear, nonlocal context. As depicted in Fig. 6, the compensator reduces the vibrations of the nonlinear system; in particular, it reduces the angular velocity oscillations significantly. Subsequently, the fluctuations of the state-dependent delay in (13) becomes small and the assumption of using constant time delay for determining the perturbed depth-of-cut in (28a) becomes more acceptable

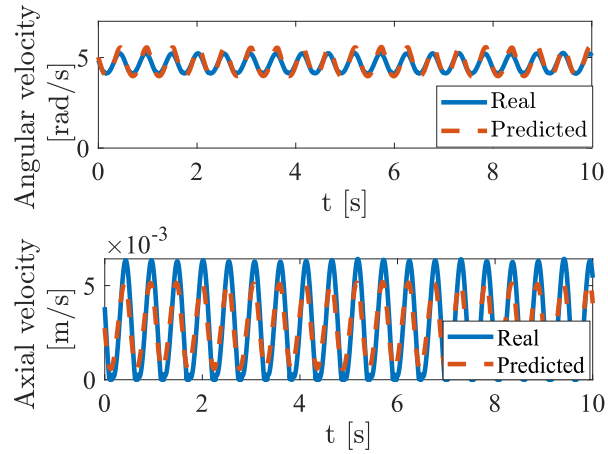

Fig. 12. Real values of the angular and axial velocities of the bit and the values estimated by the predictor.

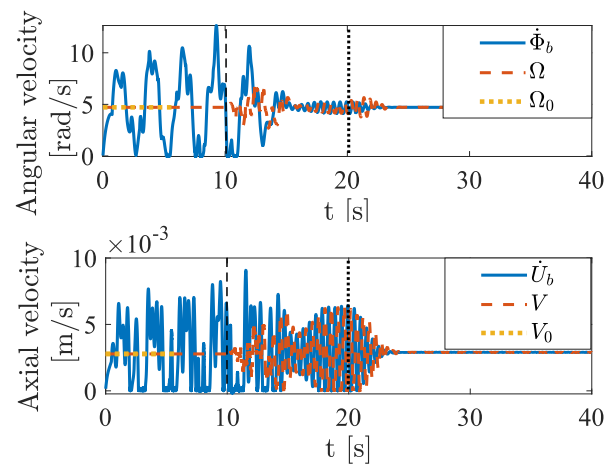

Fig. 13. Closed-loop behavior of the nonlinear dynamics. The dashed and dotted lines indicate the time instant at which, respectively, the compensator and the predictor-based controller are turned on.

(than the uncompensated case). For the compensated nonlinear system, the time evolution of the angular and axial velocities of the bit, and the predicted time evolution of these variables by the predictor are depicted in Fig. 12. Although there is some discrepancy between the real and the predicted values, especially for the axial velocity, the predictor (which was based on the linearized dynamics) still provides acceptable performance in the nonlinear case.

Now, let us apply the predictor-based controller to the nonlinear system dynamics. Fig. 13 shows the behavior of the nonlinear dynamics after applying the compensator at the time $t = 10$ s and then, applying the predictor-based controller at the time $t = 20$ s. It is observed that after applying the predictor-based controller, the vibrations are completely mitigated, which shows the effectiveness of the proposed control approach for stabilizing the original nonlinear system. In addition, both the amplitude and frequency content of the control inputs (angular and axial velocities of the top drive, indicated by the red lines in the figure) are such that real-life implementation is feasible.

It should be noted that in more harsh drilling conditions, e.g., drilling a harder rock formation or drilling with a higher

nominal rate of penetrations, the amplitude of the angular oscillations may be relatively high even after applying the compensator. In this case, the difference between the behavior of the system and the predicted behavior of the linearized system may become considerable. In such scenarios, the applicability of the prediction-based controller may reach its limits. Moreover, when the uncertainty in the bit–rock parameters grows to more extreme levels, the prediction error may also increase and reduce the effectiveness of the controller. Another crucial parameter that influences the performance of the controller is the drill-string length. In drill strings with very high length, the input delay in the dynamics in (9) is large, resulting in higher prediction errors, and consequently, a potential reduction in the efficiency of the controller.

VI. Conclusion

This article has presented a novel control design methodology for the mitigation of undesired axial and torsional vibrations of a distributed drill-string system. The coupled axial–torsional dynamics of the drill string have been represented in terms of an NDDE. Formulating the system dynamics in a lower-order state-space model has eliminated the requirement for an observer and has simplified the controller design, compared to controllers in the literature. By employing a novel precompensator, a transformation has been introduced to embed the neutral terms in the control inputs and present the open-loop dynamics in the RDDE framework rather than the NDDE framework. A criterion is developed to ensure that the right-most pole is located in a prescribed left-half complex plane, ensuring a guaranteed exponential decay rate. Based on this criterion, a parametric controller has been designed in analytic form (depending directly on drill-string system parameters), not requiring a numerical redesign of the controller when the system parameter values change. By a simulation-based case study, it has been shown that the proposed controller stabilizes the drilling system, which is unstable for the selected field parameters, with the prescribed decay rate. Furthermore, the controller is capable to mitigate undesired vibrations of the original nonlinear model and it is robust again parametric uncertainties in the bit–rock interaction.

Appendix

A. Definitions

Definition 1 [61]: K^* is the fundamental matrix of (73) if it satisfies the following equation:

$$\frac{dK^*}{d\hat{t}}(\hat{t}) = A_0K^*(\hat{t}) + A_1K^*(\hat{t}-\hat{\tau}_0) \tag{78}$$

with $K^*(0) = 0_{n\times n}$ and $K^*(\hat{t}) = I_{n\times n}$, where $0_{n\times n}$ and $I_{n\times n}$ are the trivial and unity matrices of degree n, respectively.

Definition 2 [43]: K^{**} is the second fundamental matrix of (73) if it satisfies the following equation:

$$\frac{dK^{**}(\hat{t})}{d\hat{t}} = (A_0+B_2K_2)K^{**}(\hat{t}) + A_1K^{**}(\hat{t}-\hat{\tau}_0) \tag{79}$$

with $K^{**}(0) = 0_{n\times n}$ and $K^{**}(\hat{t}) = I_n\times_n$, where $0_{n\times n}$ and $I_{n\times n}$ are the trivial and unity matrices, respectively.

Now consider the initial value problem

$$\frac{dX(\hat{t})}{d\hat{t}} = (A_0+B_2K_2)X(\hat{t}) + A_1X(\hat{t}-\hat{\tau}_0), \quad \hat{t}\geq 0 \tag{80a}$$

$$X(\theta) = K^*(\mu+\theta), \quad \theta\in[-\hat{\tau}_0, 0]. \tag{80b}$$

The unique solution of (80) is given by

$$X(\hat{t},\mu) = K^{**}(\hat{t})K^*(\mu) + \int_{-\hat{\tau}_0}^{0} K^{**}(\hat{t}-\hat{\tau}_0-\theta)A_1K^*(\mu+\theta)d\theta. \tag{81}$$

The following variabels are introduced based on the fundamental matrix (78), the solution (81), and the gain matrices (50) to be used for predictor-based control design in Section IV:

$$\begin{aligned} Q_v(\hat{t}) &= K_2K^*(\hat{t}) \\ Q_w(\hat{t}) &= K_1X(\hat{\tau}_t-\hat{\tau}_a,\hat{t}). \end{aligned} \tag{82}$$

B. Lemmas

Lemma 1: For positive values $b>\nu>0$, $\min|\lambda+b|_{\lambda\in D} = b-\nu$, where $D=\{\lambda|\mathrm{Re}(\lambda)\geq-\nu\}$.

Proof: Since $\mathrm{Re}(\lambda)\geq-\nu$, we can write $\mathrm{Re}(\lambda) = -\nu+\alpha+\beta i$ where α is a nonnegative real number and β is a real number. Hence, for $\lambda\in D$

$$|\lambda+b| = \sqrt{\left(\mathrm{Re}(\lambda)+b\right)^2+\mathrm{Im}(\lambda)^2} = \sqrt{(b-\nu+\alpha)^2+\beta^2} \tag{83}$$

where

$$\min\sqrt{(b-\nu+\alpha)^2+\beta^2}_{\alpha\geq0,\beta} = b-\nu \tag{84}$$

which completes the proof of the statement of the lemma. □

Lemma 2: The maximum magnitude of the complex function $g(\lambda) = ((1-e^{\hat{\tau}_0\lambda})/\lambda)$ in the region $D=\{\lambda|\mathrm{Re}(\lambda)\geq-\nu\}$, with $\hat{\tau}_0,\nu>0$, is not larger than $((1+e^{-\hat{\tau}_0\nu})/\nu)$.

Proof: Let us divide the region D into two subregions, inside and outside the circle $|\lambda|=\nu$: $D_1=\{\lambda||\lambda|\leq\nu\}$, and $D_2=\{\lambda|\mathrm{Re}(\lambda)>-\nu\wedge|\lambda|>\nu\}$, respectively. Since $\lim_{\lambda\to0}g(\lambda) = -\hat{\tau}_0$, the origin is a removable singular point for $g(\lambda)$, and the function $g(\lambda) = ((1-e^{\hat{\tau}_0\lambda})/\lambda)$, (with defining $g(0) = -\hat{\tau}_0$) can be considered as an analytic function. Hence, according to the maximum modulus principle in complex analysis, its maximum magnitude in the region D_1 corresponds to a point located on its boundary, $|\lambda|=\nu$

$$\begin{aligned} \max\left|\frac{1-e^{\hat{\tau}_0\lambda}}{\lambda}\right|_{\lambda\in D_1} &= \max\left|\frac{1-e^{\hat{\tau}_0\lambda}}{\lambda}\right|_{|\lambda|=\nu} \\ &\leq \frac{1+\max|e^{\hat{\tau}_0\lambda}|_{|\lambda|=\nu}}{\min|\lambda|_{|\lambda|=\nu}} = \frac{1+e^{\nu\hat{\tau}_0}}{\nu}. \end{aligned} \tag{85}$$

In addition,

$$\sup|e^{-\hat{\tau}_0\lambda}|_{\lambda\in D_2} = e^{\sup\left(\mathrm{Re}(-\hat{\tau}_0\lambda)\right)_{\lambda\in D_2}} = e^{\nu\hat{\tau}_0}. \tag{86}$$

Hence, the following relation holds:

$$\sup\left|\frac{1-e^{\hat{\tau}_0\lambda}}{\lambda}\right|_{\lambda\in D_2} \leq \frac{1+\sup|e^{\hat{\tau}_0\lambda}|_{\lambda\in D_2}}{\nu} = \frac{1+e^{\nu\hat{\tau}_0}}{\nu}. \tag{87}$$

As a result

$$\max \left| \frac{1 - e^{\hat{\tau}_0 \lambda}}{\lambda} \right|_{\lambda \in D} \leq \frac{1 + e^{\nu \hat{\tau}_0}}{\nu}. \tag{88}$$

□

References

[1] K. Rappold, "Drillstring vibration measurements detect bit stick-slip," *Oil Gas J.*, vol. 91, no. 9, pp. 66–70, 1993.

[2] W. Wu, G. Jiang, S. Huang, and C. J. Leo, "Vertical dynamic response of pile embedded in layered transversely isotropic soil," *Math. Problems Eng.*, vol. 2014, pp. 1–12, Jan. 2014.

[3] V. Vaziri, M. Kapitaniak, and M. Wiercigroch, "Suppression of drill-string stick–slip vibration by sliding mode control: Numerical and experimental studies," *Eur. J. Appl. Math.*, vol. 29, no. 5, pp. 805–825, Oct. 2018.

[4] E. Detournay and P. Defourny, "A phenomenological model for the drilling action of drag bits," *Int. J. Rock Mech. Mining Sci. Geomech. Abstr.*, vol. 29, no. 1, pp. 13–23, Jan. 1992.

[5] R. W. Tucker and C. Wang, "Torsional vibration control and Cosserat dynamics of a drill-rig assembly," *Meccanica*, vol. 38, no. 1, pp. 145–161, 2003.

[6] M. A. Trindade and R. Sampaio, "Active control of coupled axial and torsional drill-string vibrations," in *Proc. 18th COBEM Int. Congr. Mech. Eng.*, 2005, pp. 1–8.

[7] T. G. Ritto, C. Soize, and R. Sampaio, "Non-linear dynamics of a drill-string with uncertain model of the bit–rock interaction," *Int. J. Non-Linear Mech.*, vol. 44, no. 8, pp. 865–876, Oct. 2009.

[8] X. Liu, N. Vlajic, X. Long, G. Meng, and B. Balachandran, "Multiple regenerative effects in cutting process and nonlinear oscillations," *Int. J. Dyn. Control*, vol. 2, no. 1, pp. 86–101, Mar. 2014.

[9] X. Liu, N. Vlajic, X. Long, G. Meng, and B. Balachandran, "Nonlinear motions of a flexible rotor with a drill bit: Stick-slip and delay effects," *Nonlinear Dyn.*, vol. 72, nos. 1–2, pp. 61–77, Apr. 2013.

[10] X. Liu, N. Vlajic, X. Long, G. Meng, and B. Balachandran, "State-dependent delay influenced drill-string oscillations and stability analysis," *J. Vib. Acoust.*, vol. 136, no. 5, pp. 051008-1–051008-9, Oct. 2014.

[11] B. Besselink, T. Vromen, N. Kremers, and N. van de Wouw, "Analysis and control of stick-slip oscillations in drilling systems," *IEEE Trans. Control Syst. Technol.*, vol. 24, no. 5, pp. 1582–1593, Sep. 2016.

[12] S. K. Gupta and P. Wahi, "Criticality of bifurcation in the tuned axial–torsional rotary drilling model," *Nonlinear Dyn.*, vol. 91, no. 1, pp. 113–130, Jan. 2018.

[13] U. J. F. Aarsnes and N. van de Wouw, "Dynamics of a distributed drill string system: Characteristic parameters and stability maps," *J. Sound Vib.*, vol. 417, pp. 376–412, Mar. 2018.

[14] T. Richard, C. Germay, and E. Detournay, "A simplified model to explore the root cause of stick–slip vibrations in drilling systems with drag bits," *J. Sound Vib.*, vol. 305, no. 3, pp. 432–456, Aug. 2007.

[15] C. Germay, V. Denoël, and E. Detournay, "Multiple mode analysis of the self-excited vibrations of rotary drilling systems," *J. Sound Vib.*, vol. 325, nos. 1–2, pp. 362–381, Aug. 2009.

[16] A. Depouhon and E. Detournay, "Instability regimes and self-excited vibrations in deep drilling systems," *J. Sound Vib.*, vol. 333, no. 7, pp. 2019–2039, Mar. 2014.

[17] X. Zheng, V. Agarwal, X. Liu, and B. Balachandran, "Nonlinear instabilities and control of drill-string stick-slip vibrations with consideration of state-dependent delay," *J. Sound Vib.*, vol. 473, May 2020, Art. no. 115235.

[18] X. Liu, X. Long, X. Zheng, G. Meng, and B. Balachandran, "Spatial-temporal dynamics of a drill string with complex time-delay effects: Bit bounce and stick-slip oscillations," *Int. J. Mech. Sci.*, vol. 170, Mar. 2020, Art. no. 105338.

[19] M. A. Faghihi, S. Tashakori, E. A. Yazdi, and M. Eghtesad, "Multiple regenerative effects of the bit-rock interaction in a distributed drill-string system," in *Recent Trends in Wave Mechanics and Vibrations*. Cham, Switzerland: Springer, 2022, pp. 491–500.

[20] E. M. Navarro-López, "An alternative characterization of bit-sticking phenomena in a multi-degree-of-freedom controlled drillstring," *Nonlinear Anal., Real World Appl.*, vol. 10, no. 5, pp. 3162–3174, Oct. 2009.

[21] Y. Liu, J. Páez Chávez, R. De Sa, and S. Walker, "Numerical and experimental studies of stick–slip oscillations in drill-strings," *Nonlinear Dyn.*, vol. 90, no. 4, pp. 2959–2978, Dec. 2017.

[22] Z. Huang, D. Xie, B. Xie, W. Zhang, F. Zhang, and L. He, "Investigation of PDC bit failure base on stick-slip vibration analysis of drilling string system plus drill bit," *J. Sound Vib.*, vol. 417, pp. 97–109, Mar. 2018.

[23] S. Tashakori and M. Fakhar, "Suppression of torsional vibrations in drilling systems by using the optimization-based adaptive backstepping controller," *Int. J. Mech. Control*, vol. 20, no. 1, pp. 105–110, 2019.

[24] T. Feng, S. Bakshi, Q. Gu, and D. Chen, "A finite element modeling framework for planar curved beam dynamics considering nonlinearities and contacts," *J. Comput. Nonlinear Dyn.*, vol. 14, no. 8, Aug. 2019, Art. no. 081003.

[25] M. G. Fernandes, E. M. Fonseca, and R. M. Natal, "Three-dimensional dynamic finite element and experimental models for drilling processes," *Proc. Inst. Mech. Eng., L, J. Mater., Des. Appl.*, vol. 232, no. 1, pp. 35–43, Jan. 2018.

[26] J. Priest, H. Ghadbeigi, S. Avar-Soberanis, and S. Gerardis, "3D finite element modelling of drilling: The effect of modelling method," *CIRP J. Manuf. Sci. Technol.*, vol. 35, pp. 158–168, Nov. 2021.

[27] D. Bresch-Pietri and M. Krstic, "Adaptive output feedback for oil drilling stick-slip instability modeled by wave PDE with anti-damped dynamic boundary," in *Proc. Amer. Control Conf.*, Jun. 2014, pp. 386–391.

[28] U. J. F. Aarsnes and N. van de Wouw, "Axial and torsional self-excited vibrations of a distributed drill-string," *J. Sound Vib.*, vol. 444, pp. 127–151, Mar. 2019.

[29] S. Tashakori, G. Vossoughi, H. Zohoor, and E. A. Yazdi, "Modification of the infinite-dimensional neutral-type time-delay dynamic model for the coupled axial–torsional vibrations in drill strings with a drag bit," *J. Comput. Nonlinear Dyn.*, vol. 15, no. 8, Aug. 2020.

[30] I. Boussaada, H. Mounier, S.-I. Niculescu, and A. Cela, "Analysis of drilling vibrations: A time-delay system approach," in *Proc. 20th Medit. Conf. Control Autom. (MED)*, Jul. 2012, pp. 610–614.

[31] M. Krstic, *Delay Compensation for Nonlinear, Adaptive, and PDE System*. Cham, Switzerland: Springer, 2009.

[32] O. J. M. Smith, "A controller to overcome dead time," *Indian Sci. Assoc. Jpn.*, vol. 6, no. 2, pp. 28–33, 1959.

[33] Z. Artstein, "Linear systems with delayed controls: A reduction," *IEEE Trans. Autom. Control*, vol. AC-27, no. 4, pp. 869–879, Aug. 1982.

[34] A. Manitius and A. Olbrot, "Finite spectrum assignment problem for systems with delays," *IEEE Trans. Autom. Control*, vol. AC-24, no. 4, pp. 541–552, Aug. 1979.

[35] W. Kwon and A. Pearson, "Feedback stabilization of linear systems with delayed control," *IEEE Trans. Autom. Control*, vol. AC-25, no. 2, pp. 266–269, Apr. 1980.

[36] M. Jankovic, "Recursive predictor design for state and output feedback controllers for linear time delay systems," *Automatica*, vol. 46, no. 3, pp. 510–517, Mar. 2010.

[37] V. L. Kharitonov, "An extension of the prediction scheme to the case of systems with both input and state delay," *Automatica*, vol. 50, no. 1, pp. 211–217, Jan. 2014.

[38] B. Zhou, "Input delay compensation of linear systems with both state and input delays by nested prediction," *Automatica*, vol. 50, no. 5, pp. 1434–1443, May 2014.

[39] V. Van Assche, M. Dambrine, J.-F. Lafay, and J.-P. Richard, "Some problems arising in the implementation of distributed-delay control laws," in *Proc. 38th IEEE Conf. Decis. Control*, Apr. 1999, pp. 4668–4672.

[40] K. Engelborghs, M. Dambrine, and D. Roose, "Limitations of a class of stabilization methods for delay systems," *IEEE Trans. Autom. Control*, vol. 46, no. 2, pp. 336–339, Mar. 2001.

[41] K. Gu, "A review of some subtleties of practical relevance for time-delay systems of neutral type," *ISRN Appl. Math.*, vol. 2012, pp. 1–46, Nov. 2012.

[42] S. Mondie and W. Michiels, "Finite spectrum assignment of unstable time-delay systems with a safe implementation," *IEEE Trans. Autom. Control*, vol. 48, no. 12, pp. 2207–2212, Dec. 2003.

[43] V. L. Kharitonov, "Prediction-based control for systems with state and several input delays," *Automatica*, vol. 79, pp. 11–16, May 2017.

[44] X. Liu, N. Vlajic, X. Long, G. Meng, and B. Balachandran, "Coupled axial-torsional dynamics in rotary drilling with state-dependent delay: Stability and control," *Nonlinear Dyn.*, vol. 78, no. 3, pp. 1891–1906, Nov. 2014.

[45] A. S. Yigit and A. P. Christoforou, "Stick-slip and bit-bounce interaction in oil-well drillstrings," *J. Energy Resour. Technol.*, vol. 128, no. 4, pp. 268–274, Dec. 2006.

[46] T. Vromen et al., "Mitigation of torsional vibrations in drilling systems: A robust control approach," *IEEE Trans. Control Syst. Technol.*, vol. 27, no. 1, pp. 249–265, Jan. 2019.

[47] T. Vromen, N. van de Wouw, A. Doris, P. Astrid, and H. Nijmeijer, "Nonlinear output-feedback control of torsional vibrations in drilling systems," *Int. J. Robust Nonlinear Control*, vol. 27, no. 17, pp. 3659–3684, 2017.

[48] D. Bresch-Pietri and F. Di Meglio, "Prediction-based control of linear input-delay system subject to state-dependent state delay—Application to suppression of mechanical vibrations in drilling," *IFAC-PapersOnLine*, vol. 49, no. 8, pp. 111–117, 2016.

[49] B. Saldivar, S. Mondié, and J. C. Á. Vilchis, "The control of drilling vibrations: A coupled PDE-ODE modeling approach," *Int. J. Appl. Math. Comput. Sci.*, vol. 26, no. 2, pp. 335–349, Jun. 2016.

[50] B. Saldivar, S. Mondié, J. J. Loiseau, and V. Rasvan, "Suppressing axial-torsional coupled vibrations in drillstrings," *J. Control Eng. Appl. Inform.*, vol. 15, no. 1, pp. 3–10, 2013.

[51] B. Saldivar, T. Knüppel, F. Woittennek, I. Boussaada, H. Mounier, and S. I. Niculescu, "Flatness-based control of torsional-axial coupled drilling vibrations," *IFAC Proc. Volumes*, vol. 47, no. 3, pp. 7324–7329, 2014.

[52] S. Tashakori, G. Vossoughi, H. Zohoor, and N. van de Wouw, "Prediction-based control for mitigation of axial–torsional vibrations in a distributed drill-string system," *IEEE Trans. Control Syst. Technol.*, vol. 30, no. 1, pp. 277–293, Jan. 2022.

[53] M. A. Faghihi, S. Tashakori, E. A. Yazdi, M. Eghtesad, and N. van de Wouw, "Suppression of axial-torsional vibrations of a distributed drilling system by the eigenvector contradiction method," *IFAC-PapersOnLine*, vol. 55, no. 36, pp. 109–114, 2022.

[54] C. Ke and X. Song, "Drilling control system using an equivalent input disturbance-based control with a neutral-type axial-torsional coupled dynamics model," *J. Dyn. Syst., Meas., Control*, vol. 141, no. 12, pp. 121013-1–121013-9, Dec. 2019.

[55] J. J. Loiseau, M. Cardelli, and X. Dusser, "Neutral-type time-delay systems that are not formally stable are not BIBO stabilizable," *IMA J. Math. Control Inf.*, vol. 19, no. 1, pp. 217–227, Mar. 2002.

[56] G. Stépán, *Retarded Dynamical Systems: Stability and Characteristic Functions*. White Plains, NY, USA: Longman, 1989.

[57] S. Dwars, "Recent advances in soft torque rotary systems," in *Proc. SPE/IADC Drilling Conf. Exhib.*, 2015, pp. 1–12, Paper SPE-173037-MS.

[58] E. Kreuzer and M. Steidl, "Controlling torsional vibrations of drill strings via decomposition of traveling waves," *Arch. Appl. Mech.*, vol. 82, no. 4, pp. 515–531, Apr. 2012.

[59] W. Michiels, "TDS Stabil: A MATLAB tool for fixed-order stabilization problems for time-delay systems," Dept. Comput. Sci., K.U.Leuven, Leuven, Belgium, Tech. Rep. TW-330, 2010.

[60] U. J. F. Aarsnes and O. M. Aamo, "Linear stability analysis of self-excited vibrations in drilling using an infinite dimensional model," *J. Sound Vib.*, vol. 360, pp. 239–259, Jan. 2016.

[61] R. Bellman and K. L. Cooke, "On the computational solution of a class of functional differential equations," *J. Math. Anal. Appl.*, vol. 12, no. 3, pp. 495–500, Dec. 1965.

Mohammad Amin Faghihi received the B.Sc. degree from Shiraz University, Shiraz, Iran, in 2015, the M.Sc. degree from the Sharif University of Technology, Tehran, Iran, in 2017, and the Ph.D. degree from Shiraz University in 2023.

He is currently a Researcher with Shiraz University. His research interests include nonlinear dynamics, vibration, control, and applied mathematics.

Shabnam Tashakori received the Ph.D. degree in mechanical engineering from the Sharif University of Technology, Tehran, Iran, in 2019.

She was a Visiting Researcher with the Eindhoven University of Technology, Eindhoven, The Netherlands, in 2018. She is currently an Assistant Professor with the Shiraz University of Technology and an Honorary Research Fellow with the University of Aberdeen, Aberdeen, Scotland. Her current research interests include (non)linear dynamics and control with applications in the drilling industry, inverse dynamics, and fractional-order systems.

Ehsan Azadi Yazdi received the B.Sc. degree from Shiraz University, Shiraz, Iran, in 2005, the M.Sc. degree from the Sharif University of Technology, Tehran, Iran, in 2007, and the Ph.D. degree from The University of British Columbia, Vancouver, BC, Canada, in 2011.

He joined the School of Mechanical Engineering, Shiraz University, in 2012, where he is currently an Associate Professor. His research interests include robust and hybrid control, and renewable energy.

Dr. Yazdi was a recipient of the Best Paper Award at the 23rd Canadian Congress of Applied Mechanics in 2011.

Hossein Mohammadi received the first B.Sc. and second B.Sc. degrees in engineering, the M.Sc. degree in applied design in mechanical engineering, and the Ph.D. degree in mechanical engineering from Shiraz University, Shiraz, Iran, in 2007, 2008, 2009, and 2013, respectively.

He received many scholar awards and became a faculty member of Shiraz University immediately after graduation, as one of the youngest assistant professors when he was 27. He has published several articles. He is also an invited reviewer of over 200 international articles in scientific journals. His research interests include, but are not limited to, machine learning, control, vibrations, dynamics, nonlinear systems, micro/nanostructures, applied mathematics, identification, modeling biomechanical systems, and robotics.

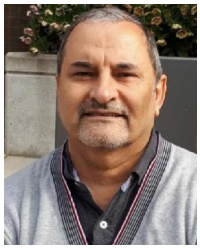

Mohammad Eghtesad received the B.Sc. and M.Sc. degrees from the University of Tehran, Tehran, Iran, in 1987 and 1989, respectively, and the Ph.D. degree from the University of Ottawa, Ottawa, ON, Canada, in 1996.

In September 1997, he started working as an Assistant Professor of mechanical engineering with Shiraz University, Shiraz, Iran, and became a Full Professor in March 2010. His engineering interests were focused on control and robotics, and he played a key role in initiating and developing research activities on control, robotics, and related research activities at the School of Mechanical Engineering, Shiraz University.

Nathan van de Wouw (Fellow, IEEE) received the M.Sc. (Hons.) and Ph.D. degrees in mechanical engineering from the Eindhoven University of Technology, Eindhoven, The Netherlands, in 1994 and 1999, respectively.

He currently holds a Full Professor position at the Mechanical Engineering Department, Eindhoven University of Technology. He has been working with Philips Applied Technologies, Eindhoven, in 2000, and the Netherlands Organisation for Applied Scientific Research, The Hague, The Netherlands, in 2001. He has been a Visiting Professor with the University of California at Santa Barbara, Santa Barbara, CA, USA, in 2006 and 2007; The University of Melbourne, Parkville, VIC, Australia, in 2009 and 2010; and the University of Minnesota, Minneapolis, MN, USA, in 2012 and 2013. He has held a (part-time) Full Professor position at the Delft University of Technology, Delft, The Netherlands, from 2015 to 2019. He has also held an Adjunct Full Professor position at the University of Minnesota from 2014 to 2021. He has published the books *Uniform Output Regulation of Nonlinear Systems: A Convergent Dynamics Approach* (Birkhauser, 2005) with A. V. Pavlov and H. Nijmeijer, and *Stability and Convergence of Mechanical Systems with Unilateral Constraints* (Springer-Verlag, 2008) with R. I. Leine.

Dr. Wouw is an IEEE Fellow for his contributions to hybrid, data-based, and networked control. He received the IEEE Control Systems Technology Award "For the development and application of variable-gain control techniques for high-performance motion systems" in 2015.